Turbidity Determination from Broadband Irradiance Measurements: A Detailed Multicoefficient Approach

CHRISTIAN A. GUEYMARD

Florida Solar Energy Center, Cocoa, Florida

(Manuscript received 30 September 1996, in final form 30 June 1997)

ABSTRACT

A physically modeled method is presented to obtain accurate turbidity determinations from broadband direct irradiance measurements. The method uses parameterizations of various extinction processes affecting the transfer of shortwave radiation in a cloudless atmosphere. The integration over the shortwave solar spectrum is performed with a more realistic weighting function than is conventionally used. The calculation and properties of the broadband aerosol optical depth are discussed in detail as a function of the aerosol optical characteristics. The method is general, as it can predict any one of the four turbidity coefficients currently used in climatological studies as defined by Ångström, Linke, Unsworth–Monteith, and Schüepp. Formal interrelationships are proposed so that climatological data based on different coefficients can be consistently intercompared without recourse to empirical formulas. The new parameterizations are more detailed than those of the literature, particularly regarding the optical depth of the clean dry atmosphere that now depends explicitly on the stratospheric ozone and nitrogen dioxide amounts. This inevitably induces changes in the prediction of the broadband turbidity coefficients (Linke and Unsworth–Monteith), particularly at small zenith angles when compared to older calculations. These coefficients are also shown to depend on zenith angle and precipitable water, causing parasitic variations of turbidity during a day or the year even if the aerosol characteristics do not vary. The masking effect of tropospheric nitrogen dioxide is presented, as well as a method to correct the predicted turbidity for circumsolar radiation. A detailed error analysis is discussed, showing that the instrumental error and the estimation error on precipitable water are the main limiting factors of the method. Although smaller potential error is obtained at larger zenith angles, accurate estimates of precipitable water are necessary for valid turbidity predictions when applied to clean dry atmospheres. A limited test of the method is presented, using spectral radiative data from five different sites as the reference. The method performs well, provided that accurate precipitable water data can be obtained. In contrast, the older Louche's method is shown to produce unrealistic negative values under clean dry conditions. Monthly average turbidity over 3–4 years was also obtained from hourly irradiance at two sites with widely different aerosol regimes. Compared to the present results, Louche's method is found to overpredict the Unsworth–Monteith coefficient at both sites, while simultaneously underpredicting the Ångström coefficient at the clearest site.

1. Introduction

Atmospheric turbidity is a convenient parameter frequently used to estimate the aerosol optical characteristics. These are important to monitor closely because of their daily, seasonal, and long-term variability, as well as their link to global climate change, atmospheric pollution, visibility degradation, and solar radiation extinction. Presently, the most accepted method of obtaining the aerosol optical depth (AOD) at different wavelengths is through the use of a multiwavelength sunphotometer. Since this method was introduced (Shaw et al. 1973; Volz 1959), it has undergone many refinements in both instrumentation and data reduction techniques (Dutton et al. 1994; Reagan et al. 1986; Shiobara et al. 1996). Absolute accuracies better than 0.002 units of AOD and relative accuracies of about 0.5% are now attainable with this method (Dutton et al. 1994; Reagan et al. 1986; Shaw 1982), at least under low to moderate aerosol loading characteristic of clean dry environments such as high-altitude sites. A recent variant of this method consists of using a multifilter rotating shadowband radiometer (MFRSR) that measures global and diffuse irradiance at various wavelengths. The direct irradiance is calculated by difference, and the corresponding AOD is finally obtained through an appropriate reduction method (Harrison et al. 1994; Harrison and Michalsky 1994). It is also possible to obtain an AOD at a far greater number of wavelengths using a spectroradiometer (Cachorro et al. 1987b; Cachorro et al. 1989; Cuomo et al. 1993), but the need for a specially designed (weatherproof and tracking) instrument together with other technical or financial considerations have apparently limited the use of this method.

Although multiwavelength sunphotometry seems the

Corresponding author address: Dr. Christian Gueymard, 2959 Ragis Rd., Edgewater, FL 32132.
E-mail: chris@fsec.ucf.edu

method of choice for accurate determination of the AOD, it also has some drawbacks. First, it is based on sophisticated and expensive instrumentation. Second, this instrumentation needs frequent and costly recalibration at remote sites where extremely low background aerosol and stable cloudless conditions are sufficiently frequent. This may explain why the world sunphotometric network is still so sparse. Operation has been sporadic and, at most, for only a few decades. Moreover, older data were typically obtained with crude single- or dual-wavelength sunphotometers. For these reasons, an alternative approach, capable of determining turbidity without these limitations, is appropriate.

This contribution will focus on the broadband (unfiltered) pyrheliometric method, which estimates aerosol turbidity in different ways from the *broadband* aerosol optical depth (BAOD). Immediate benefits of this broadband approach are twofold. The relatively inexpensive, yet accurate instrumentation to be used is part of a monitoring network that is considerably more dense than its sunphotometric counterpart. Moreover, high-quality historic data started in the 1880s (e.g., Roosen et al. 1973; Stothers 1996). The prospect of using such extensive data series or a large number of datasets from very diverse sites is particularly appealing in the context of climatological studies related to long-term climate change, volcanic activity, or pollution trends.

The origin of the broadband turbidity method can be traced to the introduction of Linke's broadband turbidity coefficient, T_L (Linke 1922), which represents the number of clean dry atmospheres (CDAs) that would be radiatively equivalent to the actual atmosphere under investigation. Subsequent improvements allowed the estimation of two spectral turbidity coefficients, Ångström's β (Ångström 1929) and Schüepp's B (Schüepp 1949), from broadband irradiance data (Louche et al. 1987; Valko 1967; Yamamoto et al. 1968). These turbidity coefficients are of spectral nature because they are defined as the aerosol optical depth at 1 and 0.5 μm, respectively. More recently, Unsworth and Monteith (1972) introduced an empirical method to obtain the BAOD from unfiltered pyrheliometric data. This is why the BAOD is also referred to as the Unsworth and Monteith turbidity coefficient. For this reason, the BAOD will be considered as a particular turbidity coefficient in what follows, even though the three other coefficients mentioned above will be calculated from it.

Turbidity estimates using experimental broadband radiometric data under selected atmospheric conditions (e.g., Bergstrom and Peterson 1977) showed promising results. A number of investigators have employed different broadband approaches using data from the meteorological network to study the local aerosol climatology at specific sites (e.g., Al-Jamal et al. 1987; Cañada et al. 1993; Fox 1994; Freund 1983; Grenier et al. 1995; Kambezidis et al. 1993; Louche et al. 1987; McGuffie et al. 1985; Polavarapu 1978; Rawlins and Armstrong 1985; Szymber and Sellers 1985; Uboegbulam and Davies 1983; Unsworth and McCartney 1973; Yamamoto et al. 1971). It is of note that the broadband approach has been shown to be useful when examining the signature of volcanic eruptions, the urban–rural pollution gradient, or the altitudinal gradient on monthly or seasonally averaged turbidity (Garrison 1995; Grenier et al. 1995; Hay and Darby 1984; Szymber and Sellers 1985; Yamashita 1974). The monthly average BAOD for 1977–90 was also estimated from measured pyrheliometric data at a number of U.S. stations and later used to predict hourly solar irradiance during the period 1961–90, constituting what is known as the National Solar Radiation Data Base (NSRDB) (Maxwell et al. 1991; Maxwell et al. 1995).

Despite its relative instrumental simplicity, consistent results from the broadband approach are difficult to obtain for several reasons. It has been continuously evolving so that basic formulations have changed over time, thus leading to method-specific turbidity values. It cannot give any precise indication of the AOD's spectral behavior without additional data. Finally, its sensitivity to parasitic factors, such as circumsolar radiation and gaseous absorption, is not well established. The present contribution addresses these factors and offers the following improvements over previous broadband methods:

- the use of a refined solar spectrum with better resolution,
- the use of recent gaseous absorption data in the determination of atmospheric extinction,
- a revised method to parameterize broadband optical depths from spectral ones,
- consideration of stratospheric and tropospheric nitrogen dioxide absorption,
- more accurate formulations for each optical mass,
- the capability of directly expressing either of two commonly used broadband turbidity coefficients (Linke and Unsworth–Monteith) as a function of more fundamental spectral ones (Ångström and Schüepp),
- a detailed error analysis, and
- a preliminary experimental test of the performance of the method under various atmospheric conditions.

2. Methodology

Contrary to all existing broadband methodologies using unfiltered pyrheliometric data, the present method uses preliminary predictions of spectral irradiance for a large range of idealized atmospheric conditions, including turbidity, which is treated here as a parametric input. After spectral integration, a parameterization of broadband irradiance is obtained from the main atmospheric variables. This relationship is simply reversed in practice to obtain turbidity from direct irradiance when the latter is measured and turbidity is the unknown. Seven individual atmospheric attenuation processes are considered here: Rayleigh scattering, absorp-

tion by ozone (O_3), stratospheric and tropospheric nitrogen dioxide (NO_2), uniformly mixed gases (UMG), water vapor, and extinction (mostly scattering) by aerosols. Following the nomenclature suggested by Horvath (1994), their respective spectral transmittances are denoted $\tau_{R\lambda}$, $\tau_{o\lambda}$, $\tau_{ns\lambda}$, $\tau_{nt\lambda}$, $\tau_{g\lambda}$, $\tau_{w\lambda}$, and $\tau_{a\lambda}$; their corresponding spectral optical depths are denoted $\delta_{R\lambda}$, $\delta_{o\lambda}$, $\delta_{ns\lambda}$, $\delta_{nt\lambda}$, $\delta_{g\lambda}$, $\delta_{w\lambda}$, and $\delta_{a\lambda}$; and their optical masses m_R, m_o, m_{ns}, m_{nt}, m_g, m_w, and m_a (the subscript λ refers to wavelength and thus denotes a spectral quantity). Within *narrow* spectral regions, these processes can be considered independent of each other, so that the total spectral transmittance for beam radiation can be obtained as a direct product of individual spectral transmittances. The incident beam spectral irradiance at normal incidence (hereafter ''beam irradiance''), $E_{bn\lambda}$, is then obtained as

$$E_{bn\lambda} = \tau_{R\lambda}\tau_{o\lambda}\tau_{ns\lambda}\tau_{nt\lambda}\tau_{g\lambda}\tau_{w\lambda}\tau_{a\lambda}E_{0n\lambda}, \quad (1)$$

where $E_{0n\lambda}$ is the extraterrestrial spectral irradiance at wavelength λ at the actual sun–earth distance. This multiplicative relationship translates into an additive one when considering the corresponding optical depths, so that the spectral AOD is given by

$$\delta_{a\lambda} = \delta_{t\lambda} - (\delta_{R\lambda} + \delta_{o\lambda} + \delta_{ns\lambda} + \delta_{nt\lambda} + \delta_{g\lambda} + \delta_{w\lambda}), \quad (2)$$

where $\delta_{t\lambda}$ is the total atmospheric spectral optical depth. The spectral AOD can be obtained from (2) if all terms on the right-hand side are known. This constitutes the usual reduction method when using sunphotometric or spectroradiometric data. Note that all optical masses have been assumed equal in (2) to simplify this presentation.

To obtain turbidity coefficients from broadband irradiance measurements, it is of considerable computational convenience to express the broadband beam irradiance, E_{bn}, in a form similar to (1):

$$E_{bn} = \tau_R\tau_o\tau_{ns}\tau_{nt}\tau_g\tau_w\tau_a E_{0n}, \quad (3)$$

where $E_{bn} = \int_0^\infty E_{bn\lambda}\, d\lambda$ and $E_{0n} = \int_0^\infty E_{0n\lambda}\, d\lambda$. The average value of E_{0n}, the ''solar constant,'' is taken here as 1367 W m^{-2}, according to the current World Meteorological Organization (WMO) recommendation. By similarity with Bouguer's equation, which, strictly speaking, is only valid for monochromatic radiation, the following equation defines the broadband transmittance for the ith attenuation process, τ_i, from the corresponding broadband optical depth, δ_i:

$$\tau_i = \exp(-m_i\delta_i), \quad (4)$$

where m_i is the optical mass for the ith process. It is stressed that, since neither the solar spectrum nor the different optical depths are constant with wavelength, each extinction process produces a unique and *airmass-dependent* signature so that the entire incoming spectrum is altered differently after its transmission through successive layers of the atmosphere. It is for this reason that even though the spectral optical depth, $\delta_{i\lambda}$, is independent of m_i, its broadband counterpart is not.

An equivalent form of (3) may then be obtained by combining it with (4):

$$E_{bn}/E_{0n} = \exp(-m_R\delta_R - m_o\delta_o - m_{ns}\delta_{ns} - m_{nt}\delta_{nt} - m_g\delta_g - m_w\delta_w - m_a\delta_a). \quad (5)$$

At the monochromatic or spectral level described by (1), the physical order of the extinction layers in the atmosphere is irrelevant. (The atmosphere is schematically considered as a succession of individual extinction layers to simplify calculations.) For large spectral bands, however, and especially for the spectrum considered as a whole, the exact order of all these extinction processes becomes significant. This is important because each layer alters the spectrum it transmits before it is incident on the next layer along the photon path. However, this correct order is not obvious a priori because both altitudinal mixing and spectral overlap occur in the real atmosphere. In particular, both water vapor absorption and aerosol extinction decrease sharply with altitude to become of secondary importance above 2–3 km. Rayleigh scattering and UMG absorption decrease monotonically with altitude through the atmosphere. Most of the O_3 absorption occurs in the stratosphere at an altitude of about 10–35 km. Finally, NO_2 is naturally present in the stratosphere in only relatively minute amounts, but it may also be present in large quantities in the lower troposphere due to air pollution. It is stressed that NO_2 absorption has been neglected in all known broadband radiation models in the literature, despite its nonnegligible effect in polluted areas. This has important consequences for the determination of turbidity, as will be shown in section 3.

A schematic description of the proposed four-layer atmosphere appears in Fig. 1. This layering scheme is such that the top absorbers (O_3 and NO_2) directly ''see'' the extraterrestrial spectrum, whereas the bottom layer (containing the aerosols) is illuminated by a spectrum modified by all the overlying layers. The top two layers constitute the CDA, which is of conceptual importance because its broadband optical depth, δ_c, does not vary appreciably with time (apart from the predictable airmass effect) and can be easily estimated. No variable stratospheric aerosol layer is considered here for simplicity because only the total aerosol column can be predicted in all broadband or sunphotometric methods, so that the stratospheric and tropospheric turbidities cannot be separated without additional measurements. Conversely to the constituents of the top layers, those of the two bottom layers are particularly variable over time. The CDA transmittance, τ_c, can be calculated from the irradiance at the bottom of an ideal clean dry atmosphere, E_c, as

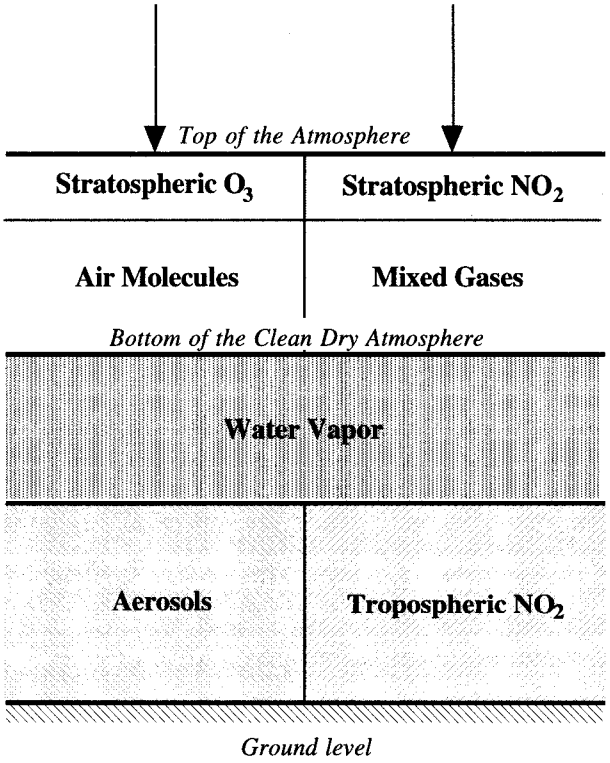

FIG. 1. Schematic representation of the extinction layers of the atmosphere.

$$\tau_c = \frac{E_c}{E_{0n}} = \frac{\int_{\lambda_0}^{\lambda_1} \tau_{o\lambda}\tau_{ns\lambda}\tau_{R\lambda}\tau_{g\lambda}E_{0n\lambda}\, d\lambda}{\int_{\lambda_0}^{\lambda_1} E_{0n\lambda}\, d\lambda}, \quad (6)$$

where λ_0 and λ_1 are the cutoff wavelengths of the pyrheliometer used to measure broadband beam radiation. The exact value of these limits of integration have been shown to have a nonnegligible impact on turbidity calculations (Thomason et al. 1982). The limits chosen here, $\lambda_0 = 280$ nm and $\lambda_1 = 4000$ nm, cover the whole sensitivity range of pyrheliometers, which are normally equipped with a quartz window. The method is also applicable to unglazed instruments because the irradiance beyond these limits is negligible. Combining (4) and (5), the *broadband* AOD is finally obtained as

$$\delta_a = (1/m_a)[\ln(E_{0n}/E_{bn}) - m_R\delta_c - m_w\delta_w - m_{nt}\delta_{nt}], \quad (7)$$

where δ_c can be recognized as $\delta_R + \delta_o + \delta_{ns} + \delta_g$. This equation can be used to obtain δ_a when E_{bn} is measured and the other variables are independently determined, as detailed below, or as also devised in previous methods (Louche et al. 1987; Maxwell et al. 1995). Because optical masses are sensitive to the actual constituent vertical density profile, (7) can be simplified by considering that the aerosol, water vapor, and tropospheric NO_2 profiles are sufficiently close to each other so that $m_w = m_{nt} = m_a$. The expressions used here for m_R and m_w as a function of the solar zenith angle, Z, are described elsewhere (Gueymard 1995; Gueymard and Kambezidis 1997):

$$m_R = [\cos Z + 0.45665Z^{0.07}(96.4836 - Z)^{-1.6970}]^{-1} \quad (8a)$$

and

$$m_w = [\cos Z + 0.031141Z^{0.1}(92.4710 - Z)^{-1.3814}]^{-1}. \quad (8b)$$

These functions do not differ much from each other and from sec$Z$ for Z below about 70°. Beyond this point, however, their difference tends to increase with Z. For instance, at $Z = 80°$, $m_R = 5.587$ and $m_w = 5.710$, whereas at $Z = 90°$, $m_R = 38.136$ and $m_w = 71.443$. Because of the way optical masses are defined, they need to be used in conjunction with the *apparent* solar zenith angle, that is, the true (astronomical) zenith angle minus refraction (Young 1974). Refraction can be calculated according to the *Astronomical Almanac* as a function of zenith angle, pressure, and temperature. Note that since the optical depths are corrected for pressure, it is unnecessary to also correct the optical masses. (Intermediate calculations have shown that replacing m_R by the absolute air mass in the nonpressure corrected optical depth parameterizations described below did not provide the correct values.)

To solve (6), its numerical integration has been performed with SMARTS2, a recent solar spectral irradiance code (Gueymard 1994b, 1995). This code evaluates the downward flux of direct and diffuse irradiance at a resolution of 1 nm between 280 and 1700 nm and 5 nm between 1705 and 4000 nm. In particular, this code offers a revised solar spectrum with higher resolution compared to simpler spectral models (e.g., Bird and Riordan 1986) and updated gaseous absorption coefficents, using recent spectrometric data mainly from Daumont et al. (1992) and Davidson et al. (1988) for the temperature-dependent O_3 and NO_2 absorption, respectively, and from MODTRAN2 (Anderson et al. 1993; Berk et al. 1989) for water vapor and mixed gas absorption. Other features include a choice of aerosol models (Braslau and Dave 1973; IAMAP 1986; Shettle and Fenn 1979) and optional calculation of the parasitic circumsolar component. (The latter is recorded as beam irradiance in the aperture of collimated radiometers; its calculation will be detailed in section 4.) Predictions with SMARTS2 have been shown to be in good agreement with those of rigorous reference codes such as MODTRAN2 and BRITE (Blättner 1983) and with high-quality experimental data measured with different spectroradiometers under a variety of atmospheric conditions (Gueymard 1995). For the present investigation, hundreds of parametric runs have been performed with SMARTS2 for varied zenith angles (0°–90°), pressure (600–1013.25 mb), O_3 thickness (0.1–0.6 atm cm or

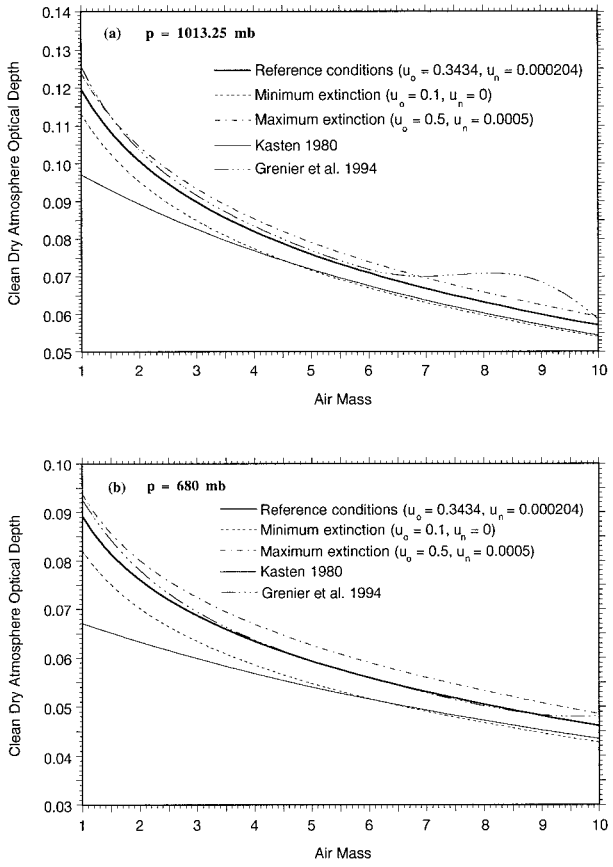

FIG. 2. Broadband optical depth of the clean dry atmosphere predicted by different methods for (a) sea level normal pressure, p = 1013.25 mb; (b) reduced pressure at 3.4-km altitude, p = 680 mb. The O_3 and NO_2 amounts, u_o and u_n, are expressed in atmospheres centimeters.

100–600 Dobson units), and stratospheric NO_2 thickness (0–0.5 matm cm). Other runs have been made to test the effect of different atmospheric vertical profiles of temperature, pressure, and gaseous abundance on δ_c. Only negligible variations around the *U.S. Standard Atmosphere* (USSA) results were obtained when considering other reference atmospheres (Anderson et al. 1986). Since the O_3 and NO_2 absorption coefficients are modeled as a function of temperature in SMARTS2, an average stratospheric temperature of −48°C (225.2 K) has been used for both. The results of these calculations have been accurately fitted, from which a manageable parameterization for δ_c has been obtained:

$$\delta_c = f_1(p, m_R)[f_2(u_o, m_R) + f_3(m_R)] + f_4(u_o, m_R) + f_5(u_n, m_R), \quad (9)$$

where f_1, f_2, f_3, f_4, and f_5 are intricate functions defined in the appendix, and u_o and u_n are the total amounts of O_3 and NO_2 in a vertical column, respectively.

Figure 2a shows the variation of δ_c with optical air mass for a sea level site where pressure p would be normal ($p = p_0$ = 1013.25 mb or 101.325 kPa) and for different atmospheric conditions: the USSA atmosphere with 0.3434 atm cm O_3 and 0.204 matm cm NO_2, an ideal atmosphere with ''minimum'' extinction (0.1 atm cm O_3 and no NO_2), and an ideal atmosphere with ''maximum'' extinction (0.5 atm cm O_3 and 0.5 matm cm NO_2). Almost all atmospheric conditions should fall between these limits. Figure 2b shows the same quantities but for an elevated site at 3.4-km altitude (p = 680 mb). This would correspond, for example, to the case of Mauna Loa, Hawaii, where solar irradiance and atmospheric turbidity measurements have been performed for extended periods. In Fig. 2, both SMARTS2-generated curves are indiscernible from those generated with MODTRAN3.5, thus adding confidence to the method. Figure 2 also compares the present method (9) to other determinations of δ_c (Grenier et al. 1994; Kasten 1980). Kasten's formula consists of a simple fit of a very old tabulation (Feussner and Dubois 1930) that has been used extensively in previous broadband turbidity calculations. The latter dataset was also reproduced in the International Geophysical Year (IGY) tables (CSAGI 1957), which were also the references for the Linke turbidity values obtained during and after the IGY. Recently, it became evident that this old tabulation was significantly too low at most air masses. This is reflected in the improved tabulations and functions that were proposed by various authors (Grenier et al. 1994; Hoyt 1975; Kasten 1996; Louche et al. 1986; Thomason et al. 1982) using different assumptions and methodologies. This improvement clearly appears in Fig. 2. However, none of these alternative expressions for δ_c explicitly accounted for O_3 or NO_2 amounts. They all neglected NO_2 and only considered a fixed amount of O_3 (0.3 atm cm), leading to seasonal systematic errors in the calculation of Linke turbidity. This is particularly true of a recently proposed expression (Grenier et al. 1994, 1995), which also suffers from an incorrect high-order polynomial fit diverging at large air masses (Fig. 2). For the comparison in Fig. 2b, the values of δ_c predicted by Kasten (1980) and Grenier et al. (1994) have been corrected for pressure instead of correcting the optical air mass as these authors propose.

The water vapor transmittance is obtained from the irradiance emanating from a clean wet atmosphere, E_w, as

$$\tau_w = \frac{E_w}{E_c} = \frac{\int_{\lambda_0}^{\lambda_1} \tau_{o\lambda}\tau_{ns\lambda}\tau_{R\lambda}\tau_{g\lambda}\tau_{w\lambda}E_{0n\lambda}\, d\lambda}{\int_{\lambda_0}^{\lambda_1} \tau_{o\lambda}\tau_{ns\lambda}\tau_{R\lambda}\tau_{g\lambda}E_{0n\lambda}\, d\lambda}. \quad (10)$$

A large number of SMARTS2 parametric runs were performed to solve (10) with the same methodology and range of atmospheric parameters as for τ_c. Since $\delta_{w\lambda}$ is modeled as a function of λ, m_w, p, and precipitable water w, in SMARTS2, the latter parameter was allowed to vary between 0 and 6 cm. As a result of these simu-

lations, δ_w was found to be largely dependent on m_w and w and also slightly on p. An accurate parameterization of δ_w is proposed in the appendix.

Using an integration method similar to (10), the tropospheric NO_2 broadband optical depth is parameterized from its total amount in a vertical column, u_{nt}, as

$$\delta_{nt} = u_{nt}[2.8669 - 0.078633 \ln^{2.36}(m_{nt})]. \quad (11)$$

The tropospheric NO_2 abundance, u_{nt}, varies considerably with weather and pollution conditions (Schroeder and Davies 1987). Typical values for u_{nt} may thus vary from near 0 to at least 0.02 atm cm for very polluted areas.

Finally, the aerosol extinction deserves a very detailed treatment because of its dependence on a number of variables. From (4), the BAOD can be defined as

$$\delta_a = (-1/m_a) \ln\tau_a, \quad (12)$$

where τ_a is the aerosol transmittance. The latter quantity can be either obtained experimentally from irradiance measurements by reversing (3) or calculated by ratioing the modeled irradiances under and above the aerosol layer for preselected atmospheric conditions. The latter option provides the necessary link between spectral information (and particularly spectral turbidity) and broadband results, without using any empirical relationship. More specifically, the aerosol transmittance is calculated here as

$$\tau_a = \frac{E_a}{E_w} = \frac{\int_{\lambda_0}^{\lambda_1} \tau_{o\lambda}\tau_{ns\lambda}\tau_{R\lambda}\tau_{g\lambda}\tau_{w\lambda}\tau_{nt\lambda}\tau_{a\lambda}E_{0n\lambda}\, d\lambda}{\int_{\lambda_0}^{\lambda_1} \tau_{o\lambda}\tau_{ns\lambda}\tau_{R\lambda}\tau_{g\lambda}\tau_{w\lambda}\tau_{nt\lambda}E_{0n\lambda}\, d\lambda}. \quad (13)$$

Different runs were performed with SMARTS2 for varying optical mass, pressure, O_3, NO_2, precipitable water, and aerosol optical characteristics to solve (13). The effects on BAOD of O_3, NO_2, and pressure around nominal values were found insignificant and were thus eliminated from the parameterization. Different aerosols were simulated, including rural, maritime, urban, tropospheric, and continental models (IAMAP 1986; Shettle and Fenn 1979), together with the common Ångström idealized model ($\delta_{a\lambda} = \beta\lambda^{-\alpha}$, where β is the aerosol optical depth at 1 μm, also known as the Ångström turbidity coefficient, and α is the wavelength exponent). For example, Fig. 3 shows the effect of β on δ_a for continental and maritime aerosols of the Standard Reference Aerosol (SRA) model (IAMAP 1986). It appears that the continental SRA produces a far larger range of δ_a with varying Z and β than its maritime counterpart. This is related to the lower average value of α in the maritime model (about 0.27) compared to the continental model (about 1.3). In the general case, and in the absence of spectral measurements, it is not possible to know a priori whether the observed aerosol layer is closer to the continental, maritime, or any other specific

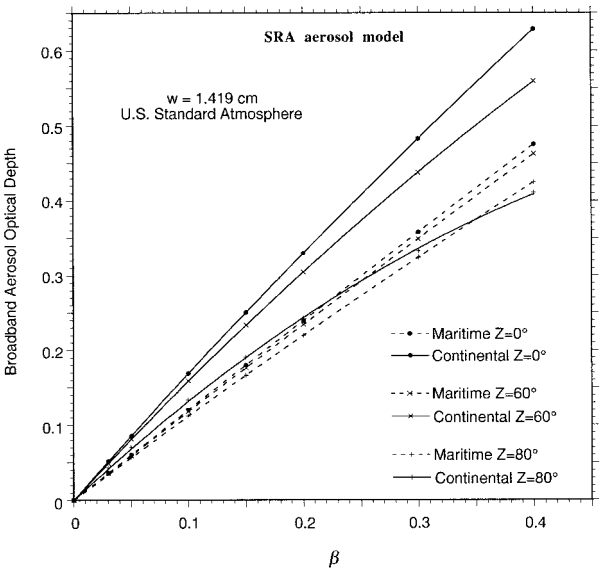

FIG. 3. Broadband aerosol optical depth for the *U.S. Standard Atmosphere* and two Standard Reference Atmosphere aerosol models: continental (continuous line) and maritime (dotted line).

model. Therefore, in the derivation that follows, only the Ångström idealized model will be investigated. Its convenience outweighs the fact that it cannot perfectly represent real aerosol spectral characteristics. It is used with a spectrally constant value of α parametrically varied between -0.5 and 2.5, and β varied between 0 and 0.4. These two wide ranges of values cover all aerosol optical characteristics that are normally observed, except under heavily sand-laden desert atmospheres where β may exceed 1.0. Figure 4 illustrates the effect of both α and β on δ_a for $w = 1.419$ cm (from the USSA) and $Z = 0°$, 60°, and 80° ($m_a = 1$, 1.998, and 5.71, respectively). It appears that δ_a is almost proportional to β when α is small. The combined effect of air mass and wavelength exponent is noticeable: for small m_a, a large effect of α on BAOD is shown in Fig. 4a. Conversely, larger values of m_a tend to ''shrink'' the spread in BAOD due to α (Fig. 4c). This can be explained by the ''reddening'' of the spectrum at large m_a. (The direct spectrum tends to shift toward longer wavelengths when the air mass increases.) At these predominantly longer wavelengths, the effect of aerosol extinction is normally far less than at shorter wavelengths, at least for $\alpha > 0$, hence the relatively small impact of α on BAOD for larger m_a.

The effect of w is particularly noticeable at large values of β, as shown in Fig. 5. The predictions obtained with the simpler and frequently used formula of Louche et al. (1987) are also shown in Fig. 5. In comparing Figs. 4 and 5, it is found that δ_a is strongly dependent on β, as would be expected, but is also significantly more affected by α than by m_a or w. The following parameterization is proposed:

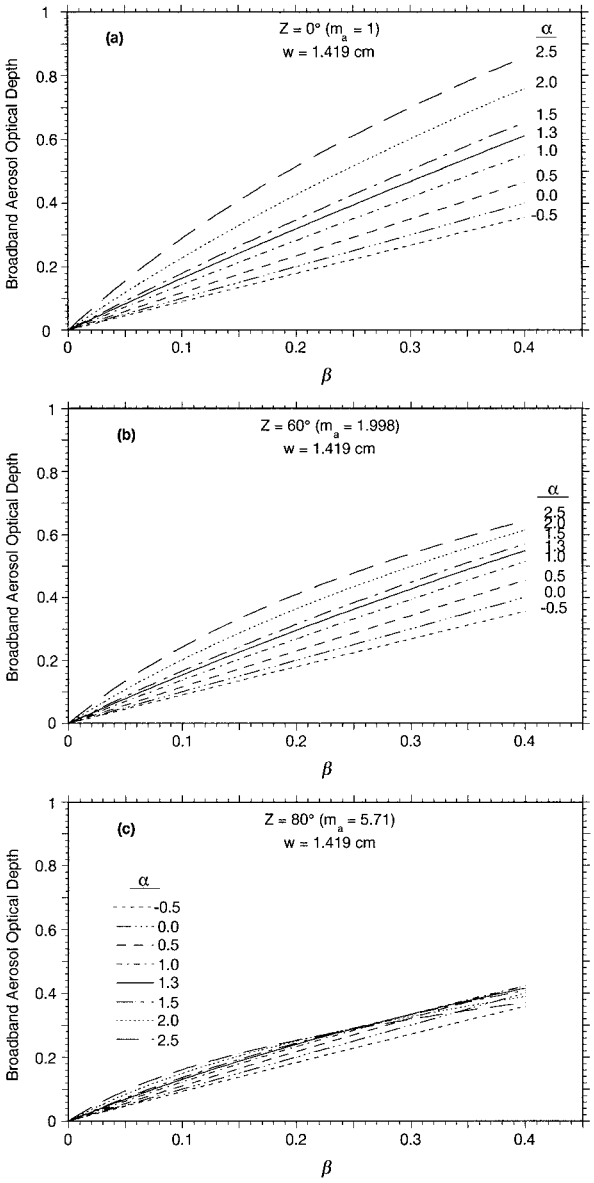

FIG. 4. Broadband aerosol optical depth for an Ångström-type aerosol, the *U.S. Standard Atmosphere*, determined as a function of β for $\alpha = -0.5$ to 2.5. (a) $Z = 0°$, (b) $Z = 60°$, and (c) $Z = 80°$.

$$\delta_a = \beta(s_1 + s_2\beta), \tag{14}$$

where s_1 and s_2 are intricate functions of the optical air mass of aerosols, m_a, and of precipitable water, w, defined in the appendix for the particular case when α is equal to its conventional value of 1.3, which is representative of aerosols of a rural–continental origin. A more complex parameterization would be necessary to accommodate the general case of a broad range of α values. However, this generalization adds another variable that tends to decrease the accuracy of the fit and is not really justified because, in most cases, α is not known a priori. Under real atmospheres, spectral or multiwavelength measurements would be necessary to obtain α, a highly variable factor that is dependent on the instantaneous aerosol size distribution. As noted previously, such measurements are considerably less frequent than broadband measurements. In those rare instances where such detailed spectral measurements are available, this broadband method would not add any significant information. However, the only way to test any broadband method is against more precise and detailed (spectral) data, as will be discussed in section 6.

An interesting limiting case is reached for $\alpha = 0$ because $\tau_{a\lambda}$ then becomes the spectrally constant value β, so that δ_a is also strictly equal to β. It follows that δ_a is more and more dependent on w as α increases. In the rare cases where α is known and differs noticeably from 1.3, a linear interpolation or extrapolation using the determinations of δ_a for $\alpha = 0$ and $\alpha = 1.3$ is possible. This is particularly so for low values of α and β and large air masses, as demonstrated by the results shown in Fig. 6.

3. Turbidity coefficients

The method proposed here is flexible since it provides a direct means of obtaining *all four* turbidity coefficients currently in use without any accuracy degradation.

a. Unsworth–Monteith turbidity coefficient

By definition (Unsworth and Monteith 1972), the Unsworth–Monteith coefficient is equal to the BAOD, δ_a. From (14), it also exhibits a dependence on both air mass and precipitable water, which should be considered parasitic because they are not characteristic of the actual aerosol loading. This means that δ_a would appear to have a slight diurnal variation even if the aerosol optical characteristics do not change. Consequently, turbidity statistics based on δ_a obtained from daytime irradiance measurements may show a different variation in aerosol content than in reality. Similarly, seasonal statistics may be contaminated by natural variations in the daily average air mass. Figure 5 shows that these parasitic variations are very significant for large values of β at even moderate values of Z but become almost negligible for $\beta < 0.05$ and $Z < 70°$. To eliminate the part of these ''virtual'' variations of turbidity caused by variations in air mass, it is possible to simply define δ_a for a reference air mass of 2 (Gueymard and Kambezidis 1997). The Unsworth–Monteith coefficient is directly obtained from (7) if all other terms are known, and thus it can be determined experimentally if E_{bn} is measured under known conditions of pressure, precipitable water, O_3, and NO_2. Equation (7) can be simplified as

$$\delta_a = (1/m_a)[\ln(E_{0n}/E_{bn}) - m_R\delta_c] - \delta_w - \delta_{nt}. \tag{15}$$

It is stressed that the tropospheric NO_2 effect is coincidentally masking a part of the aerosol effect (see also Gueymard and Kambezidis 1997). Tropospheric

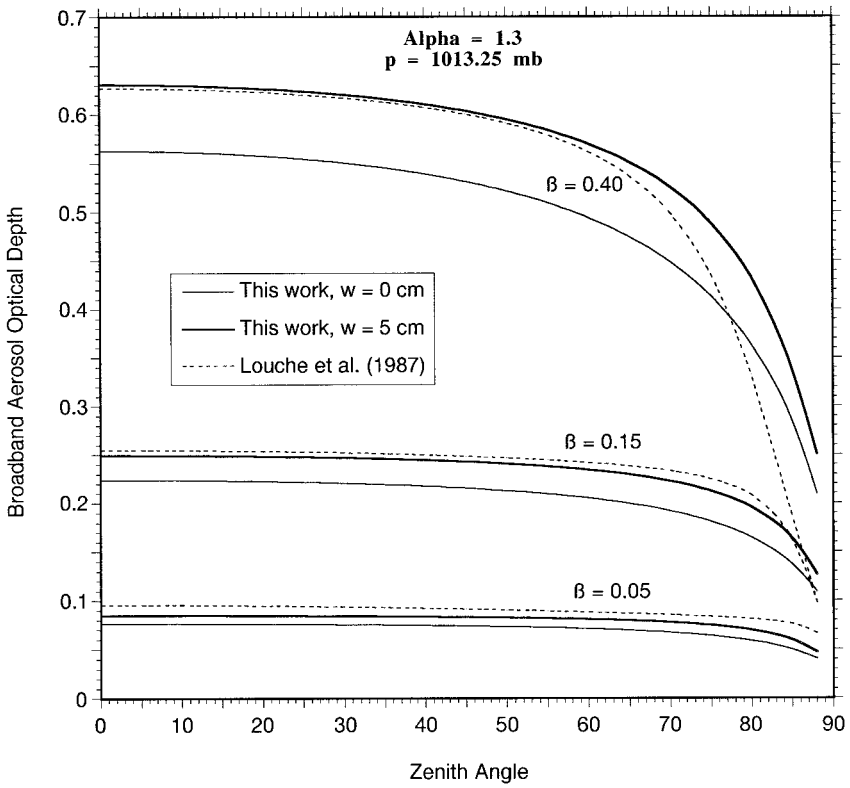

FIG. 5. Broadband aerosol optical depth as a function of Z for an Ångström-type aerosol and the *U.S. Standard Atmosphere,* as determined by different methods for $\alpha = 1.3$ and $w = 0$ or 5 cm.

NO_2 absorption has a parasitic effect on turbidity because the former cannot be discriminated from the latter unless specialized measurements of NO_2 abundance (total column) are available, which is rare. The NO_2 effect may not be negligible in urban areas, but, because τ_{nt} is generally an unknown in (15) and is therefore assumed to be zero, an overestimation, of equal magnitude, of δ_a results. For example, suppose that E_{bn} is measured to be 1000 W m^{-2} at the average sun–earth distance ($E_{0n} = 1367$ W m^{-2}) and for a zenith sun ($m_R = m_a = 1$) under the following atmospheric conditions: $p = 1013.25$ m, $u_o = 0.35$ atm cm, $u_{ns} = 0.2$ matm cm, $u_{nt} = 10$ matm cm, and $w = 1$ cm. Under this scenario, the following results are obtained from (9) through (15): $\delta_c = 0.1197$, $\delta_w = 0.1119$, $\delta_{nt} = 0.0287$, and $\delta_a = 0.0522$. Neglecting both tropospheric and stratospheric NO_2 would yield $\delta_c = 0.1191$ and $\delta_a = 0.0815$. This latter result translates into a considerable 56% overestimation of the pure BAOD in this ideal example.

b. Linke turbidity coefficient

The Linke coefficient, T_L, is equivalent to the number of clean dry atmospheres needed to radiatively equal the real atmosphere. This translates into

$$E_{bn} = E_{0n} \exp(-m_R \, \delta_c \, T_L). \qquad (16)$$

Eliminating E_{bn} and E_{0n} from (15) and (16), a relationship between T_L and δ_a is readily obtained:

$$T_L = 1 + (m_a/m_R)(\delta_w + \delta_{nt} + \delta_a)/\delta_c. \qquad (17)$$

The main problem with T_L is that it is not a pure turbidity coefficient because it also incorporates the water vapor and NO_2 optical depths. Moreover, it is subject to virtual daily variations like δ_a due to the combination of different parasitic effects. This is demonstrated in Fig. 7 where T_L is plotted for the same set of atmospheric parameters as in Fig. 5. Virtual variations due to Z alone are smoother than those of δ_a for $Z < 80°$ but become steeper for larger zenith angles. To remove a part of T_L's parasitic variation, it is advisable to calculate it for a reference airmass value of 2 (Grenier et al. 1994; Kasten 1988). The water vapor effect is, however, the dominant issue here. For instance, it appears from Fig. 7 that the same value of T_L (3.08) corresponds to either $\beta = 0.05$ and $w = 5$ cm or $\beta = 0.15$ and $w = 0$ cm.

The combination of (14) and (17) allows an easy and consistent determination of T_L when β is known or vice versa. Before that, empirical fits were necessary to intercompare T_L and β (Abdelrahman et al. 1988; Dogniaux 1986, 1994; Grenier et al. 1994; Hinzpeter 1950; Katz et al. 1982; WMO 1981). Equation (30) of Grenier et al. (1994) has been chosen here as a typical representation of these simple relationships and is shown in Fig. 7. Clear-

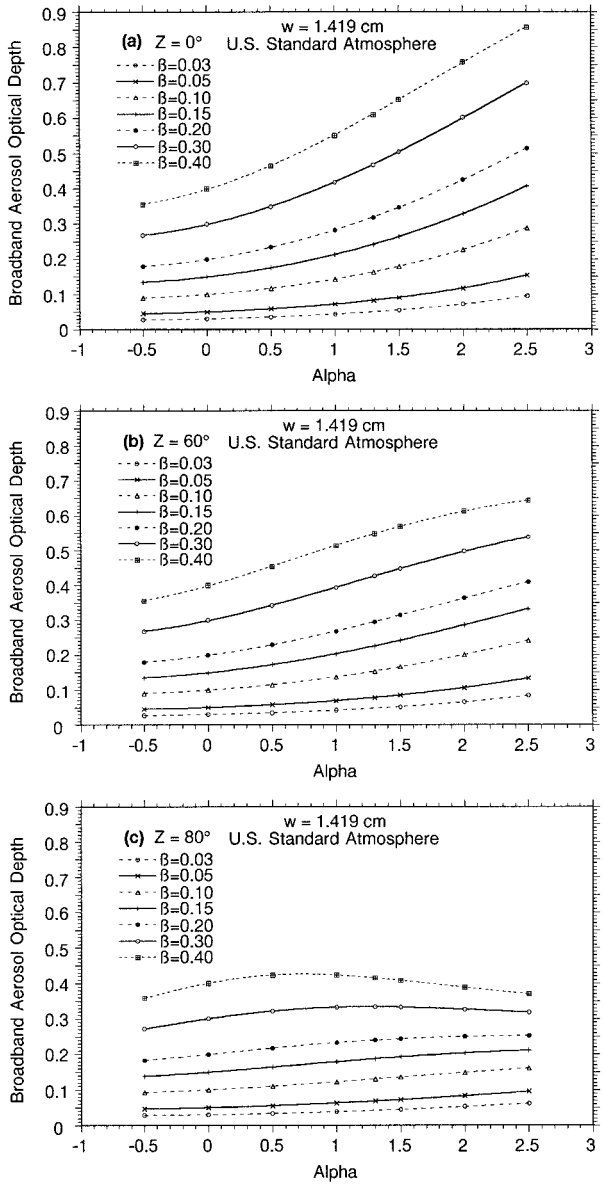

FIG. 6. Broadband aerosol optical depth for an Ångström-type aerosol and the *U.S. Standard Atmosphere*, as determined as a function of α. (a) $Z = 0°$, (b) $Z = 60°$, and (c) $Z = 80°$.

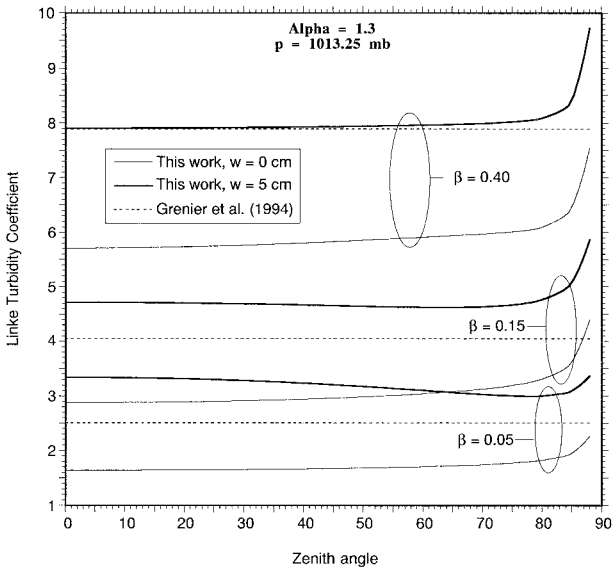

FIG. 7. Linke turbidity coefficient determined by different methods as a function of *Z*, β, and *w*.

ly, it can estimate T_L with acceptable accuracy only if *w* is around 2 cm, β is low or moderate, and $Z < 80°$. Due to this large dependence of T_L on *w*, among other factors, the use of T_L should be discouraged in favor of δ_a, as also recommended elsewhere (Gueymard and Kambezidis 1997; Molineaux and Ineichen 1996), or, even better, in favor of a spectral turbidity coefficient (see next section). Under the idealistic scenario detailed above, T_L would be 2.611 or 2.624 when neglecting NO_2. Interestingly, the calculated T_L using Kasten's expression for δ_a would yield $T_L = 3.22$. The large difference obtained between Kasten's T_L predictions and those of (17) is likely to be less at larger air masses because of the smoother slope of Kasten's δ_c (Fig. 3).

c. Ångström and Schüepp turbidity coefficients

The Ångström and Schüepp turbidity coefficients, β and *B*, both have a spectral definition; namely, they correspond to the AOD at 1 μm (base e) and 0.5 μm (base 10), respectively, and for this reason they are *true* turbidity coefficients not affected by anything else than the aerosol total burden. *If* an aerosol respects Ångström's idealized model, the uses of β or *B* are strictly equivalent and choosing one or the other is only a matter of convenience.

Once δ_a is evaluated using the method described earlier in this section, Ångström's β coefficient can be calculated by solving (14), giving

$$\beta = (s_1/s_2)[-1 + (1 + 4s_2\delta_a/s_1^2)^{1/2}]/2, \qquad (18)$$

where δ_a is obtained from (15).

In the general case, both s_1 and s_2 in (18) depend on the wavelength exponent α. As discussed earlier, β cannot be evaluated unless α is known a priori. This uncertainty in α makes the determination of β less precise and discriminating, despite the fact that β, unlike δ_a or T_L, is a true turbidity coefficient. As an alternative, it has therefore been suggested (Gueymard 1994a) to report β^*, the reduced value of β with α fixed at the conventional value of 1.3. For the numerical example in section 3a, a value of $\beta^* = 0.0319$ is obtained with the present method when accounting for NO_2 absorption. When this absorption is neglected, the apparent β^* increases to 0.0499, a 56% overestimation.

Finally, Schüepp's *B* coefficient is easily calculated from β, using their respective definitions:

TABLE 1. Optical geometry of some typical pyrheliometers (degrees). * Normal incidence pyrheliometer. ** Linke–Feussner.

Pyrheliometer type	Slope angle	Opening angle	Limit angle
Abbott silver disk	0.8	2.9	4.9
Eppley NIP*	1.78	2.91	4.03
Eppley H–F	0.804	2.50	4.19
Kipp and Zonen L–F**	1.0	5.08	9.11
Kipp and Zonen CH1	1.0	2.5	4.0

$$B = 2^{\alpha}\beta/\ln 10, \tag{19}$$

which, for $\alpha = 1.3$, translates into $B^* = 1.069\beta^*$. Other relationships between B and δ_a or T_L may be obtained by combining (18) with (19), or substituting (14) into (17) and combining with (19). This eliminates the need for empirical expressions (e.g., Valko 1967).

4. Circumsolar radiation

So far, all derivations were made considering that only true beam radiation was entering the pyrheliometer's aperture. In practice, such instruments have a nonnegligible field of view. This makes them also responsive to the diffuse radiation emanating from the bright aureole, which is caused by aerosol-induced scattering around the solar disk. Whereas most current instruments have an aperture of 4°–6°, some older instruments had considerably larger apertures, for example, 10°–15° (Ångström 1961; Ångström and Rodhe 1966; Pastiels 1959). In reality, more radiation than expected is measured by the instrument, and thus the basic calculation described in the previous section tends to slightly *underestimate* turbidity. The magnitude of this underestimation depends on the parasitic diffuse irradiance intercepted, which, in turn, is largely a function of the solar zenith angle and the optical depth and phase function of the aerosol. It is stressed that this circumsolar effect is normally low under most conditions but may become important if at least one of the following circumstances arises: large air mass, large pyrheliometer aperture, heavy aerosol loading, or large aerosol such as maritime particulates or wind-blown desert dust. The need for correcting pyrheliometric output for circumsolar radiation has been recognized early because of its parasitic effect during instrumental intercomparison studies (e.g., Ångström 1961; Pastiels 1959). However, no specific method seemed to have been proposed to systematically correct direct irradiance data or broadband turbidity for circumsolar effects.

Calculations of broadband circumsolar radiation have been performed here with the SMARTS2 code for different pyrheliometer geometries and two different aerosol models: the continental and maritime SRA. The spectral circumsolar calculations in SMARTS2 are based on an approximation of multiple scattering (Box and Deepak 1979, 1981). Discrete spectral calculations of phase functions (Putsay 1995a,b) obtained with a Mie code have been fitted as a continuous function of the scattering angle and wavelength. The parasitic broadband circumsolar irradiance, E_{dc}, is obtained as

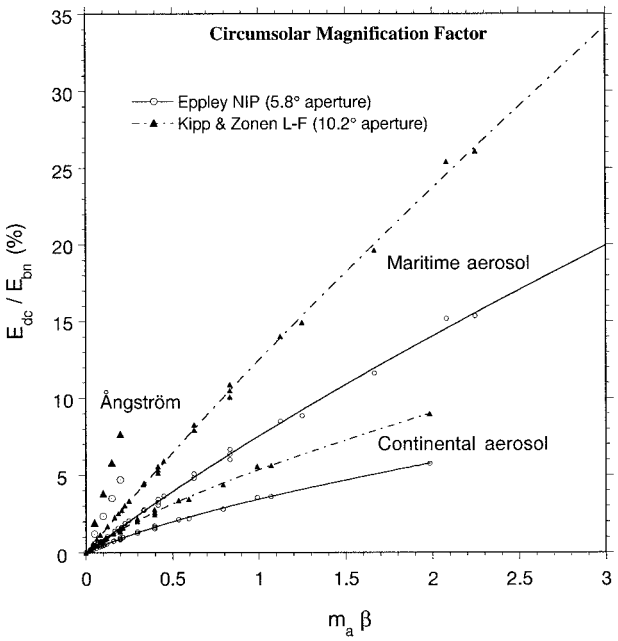

FIG. 8. Circumsolar magnification factor, or percent circumsolar radiation added to the true direct irradiance, for SRA's continental and maritime aerosols and two different pyrheliometers (Eppley NIP and Kipp and Zonen Linke–Feussner), obtained from either (20) or Ångström (1970).

$$E_{dc} = 2\pi \int_{\lambda_0}^{\lambda_1} \int_0^{\varepsilon} L_{\lambda}(\xi) P(\xi) \sin\xi \cos\xi \, d\xi \, d\lambda, \tag{20}$$

where ξ is the scattering angle, ε is the limit angle of the pyrheliometer, $L_{\lambda}(\xi)$ is the sky radiance along the almucantar, and $P(\xi)$ is the penumbra function [a purely geometric characteristic of the pyrheliometer, varying between $P(0) = 1$ and $P(\varepsilon) = 0$]. Five widely used pyrheliometers have been specifically considered for this analysis because they are characteristic of both old and recent measurements. Their geometry (slope angle, opening angle, and limit angle, as defined in the radiometric literature, e.g., Ångström 1961) was obtained from different sources (Ångström 1961; Major 1994; Pastiels 1959; Zerlaut 1983) and appears in Table 1. These three characteristic angles are necessary to obtain the penumbra function (Major 1994; Pastiels 1959). Once E_{dc} is obtained from (20), a circumsolar magnification factor (CMF) is defined as $F_c = 100\, E_{dc}/E_{bn}$.

Sample results of these calculations appear in Fig. 8 for two widely used instruments: the Eppley ''Normal Incidence Pyrheliometer'' and Kipp and Zonen ''Linke–Feussner Actinometer.'' As might be expected, the latter instrument, with an aperture (or twice the opening angle) about 70% larger than that of the former, has a larger CMF of roughly the same proportion. Moreover, for

TABLE 2. Coefficients for (21). The numbers in the first row apply to a continental aerosol, and those in the second row (within brackets) apply to a maritime aerosol. * Normal incidence pyrheliometer. ** Linke–Feussner.

Pyrheliometer type	$a0$	$a1$	$a2$	$b0$	$b1$	$b2$
Abbott silver disk	6.001	277.88	60.979	9.0017	16.957	173.56
	(8.5011)	(254.02)	(32.438)	(2.0017)	(−0.99002)	(50.706)
Eppley NIP*	7.0013	484.44	98.802	9.0023	10.183	171.66
	(9.0547)	(329.09)	(37.989)	(1.9019)	(−0.7348)	(48.235)
Eppley H–F	4.7514	96.836	24.042	9.0008	30.265	190.10
	(7.3012)	(543.41)	(78.542)	(2.1016)	(−0.43503)	(52.859)
Kipp and Zonen L–F**	14.002	790.85	101.51	11.004	−3.1631	159.05
	(16.901)	(1421.2)	(103.16)	(1.7515)	(−1.3677)	(52.636)
Kipp and Zonen CH1	5.4007	276.34	66.441	9.002	16.043	170.04
	(8.9015)	(619.22)	(73.891)	(1.852)	(−0.69325)	(47.324)

either instrument, the maritime aerosol model used here generates about 2.5 times more circumsolar radiation than its continental counterpart because of a sharper phase function. Figure 8 also shows that the older calculations performed by Ångström (Ångström and Rodhe 1966; Ångström 1970) produced far larger CMFs, possibly due to their semiempirical derivation (the aerosol optical characteristics were not mentioned but were presumably close to the continental model) and a lack of accurate coincident turbidity data. Note that the present method can be extended to instruments with similar geometries through interpolation and to instruments equipped with a noncircular aperture using intermediate calculations (Ångström and Rodhe 1966).

Results of numerous evaluations of (20) for a large range of turbidities and air masses have been parameterized through

$$F_c = [(a_0 + a_1\beta)m_a\beta/(1 + a_2\beta)] \times [1 + (b_0 + b_1\beta)m_a\beta/(1 + b_2\beta)], \quad (21)$$

where coefficients a_i and b_i are given in Table 2 for each pyrheliometer geometry and aerosol model. The difficulties in evaluating F_c are twofold. First, it depends on β, which is precisely the main unknown. Second, it depends sharply on the spectral variation of the aerosol phase function and scattering optical depth, which are also unknown most of the time. It is therefore suggested to use F_c for the *continental aerosol* as a default because it is most common over land and to use F_c for the maritime aerosol only in cases where evidence suggests that the presence of such aerosol is more likely. Using the continental aerosol model underestimates the true F_c if the real aerosol is of maritime or desertic origin. Conversely, this assumption will overestimate F_c if the real aerosol is sulfate-rich of urban origin. A simple way to overcome the former problem is to obtain a preliminary estimate of AOD, δ_{a0}, through (15), considering first that no circumsolar radiation is present. Equation (18) then provides the preliminary evaluation of β, which can be imported into (21), providing F_c. The incremental correction on δ_a caused by circumsolar radiation is then $d\delta_a = \ln(1 + F_c/100)/m_a$. The new estimate of the BAOD is now $\delta_{a1} = \delta_{a0} + d\delta_a$. The process can normally be stopped here or iteratively repeated if a large circumsolar correction is anticipated.

5. Error analysis

Both the spectral and broadband methods calculate the aerosol optical depth by subtracting different known quantities from a measured total optical depth. However, with the broadband approach, it is not possible to avoid the interference caused by strong water vapor absorption. It is therefore expected that any important error in the estimation of precipitable water will affect δ_a, T_L, β, and B. Using Bevington's approach (Bevington 1969), the probable absolute error in δ_a can be obtained from

$$\Delta\delta_a = \left\{\left(m_a^{-1}\frac{\Delta E_{bn}}{E_{bn}}\right)^2 + \left(\frac{m_R}{m_a}\right)^2\left[\left(\frac{d\delta_c}{du_o}\Delta u_o\right)^2 + \left(\frac{d\delta_w}{dw}\Delta w\right)^2\right] + \left(\frac{d\delta_{nt}}{du_{nt}}\Delta u_{nt}\right)^2\right\}^{1/2}. \quad (22)$$

The first term on the right-hand side of (22) corresponds to the instrumental error, which is estimated to be 0.1%–3% in very well-maintained monitoring systems. The three remaining errors are due to inaccuracies in either the modeling process or the input data. No significant inaccuracy is expected from the extraterrestrial irradiance, the site's pressure, the CDA modeling (apart from the ozone influence), or the air mass since time is assumed to be carefully recorded and the instantaneous zenith angle is assumed to be calculated correctly. Mod-

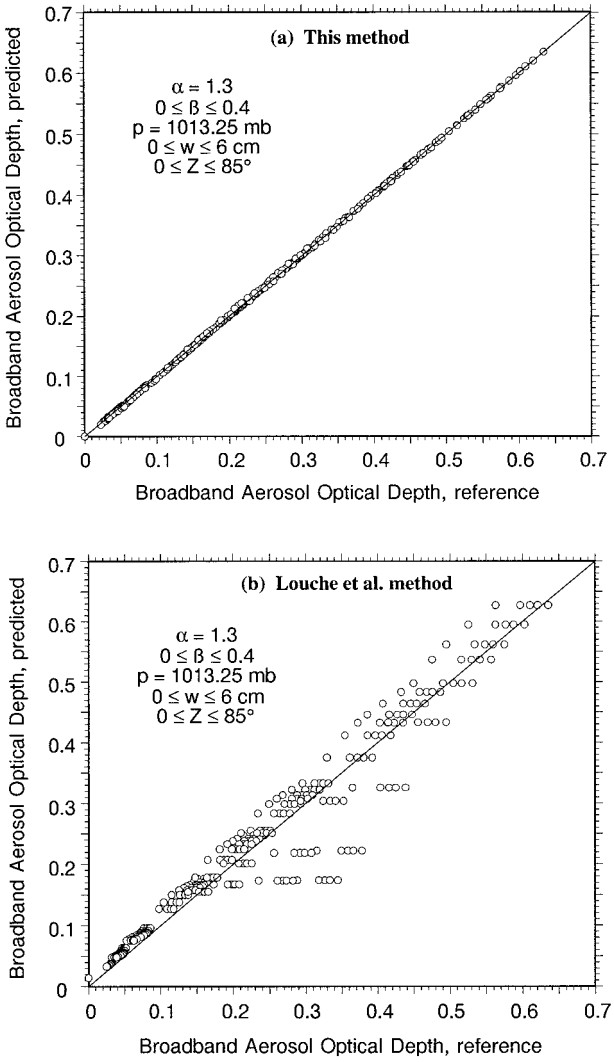

FIG. 9. Predicted vs reference broadband aerosol optical depth for (a) this method and (b) the method of Louche et al. (1987).

eling errors have been kept to a minimum on the order of 0.1%–0.5% in most cases. This is illustrated in Fig. 9a for a large range of atmospheric conditions with remarkably good agreement between the predicted values from (14) and the original values obtained from direct spectral integration. The root-mean-square error (rmse) of the predictions is 0.6% of the average δ_a for this example. (Obviously, any error in the original spectral code would not be accounted for here.) Conversely, Fig. 9b shows that the commonly used method of Louche et al. (1987) may have very significant deviations from the ideal 1:1 correspondence with an rmse of 17%.

The effect of the remaining three terms on the right-hand side of (22) is now investigated in detail. The error in δ_a caused by a relative input error of 20% in the amounts of O_3 or NO_2 is generally small and decreases slightly with increasing Z: the first and third term (unsquared) are less than 0.003 if $u_o < 0.4$ atm cm and $u_{nt} < 5$ matm cm. The error in δ_a caused by a similar input error in w can be much larger, depending on w and Z. Table 3 summarizes the results obtained for $\Delta\delta_a$ from (22) for $Z = 10°$, 30°, 60°, and 80°; $p = 1013.25$ mb; $u_o = 0.3$ atm cm; $u_{nt} = 1$ matm cm; and w varying between 0.1 and 5 cm. The inputs of u_o, u_{nt}, and w are subject to a relative error of 20%, and the instrumental error is either 0.5% or 3%. Similar calculations are also provided for an input error of 100% on w and 20% error on u_o and u_{nt}. This latter case is certainly rare for very moist atmospheres (e.g., $w > 1.5$ cm) but may be frequent for very dry atmospheres ($w < 0.5$ cm) whenever w needs to be estimated from surface data or from climatological data. The results show that $\Delta\delta_a$ decreases significantly with increasing Z because the instrumental error [the first term of the right-hand side in (22)] is dominant, at least at small zenith angles or small relative errors on w, and it is divided by the aerosol optical mass. It follows that irradiance measured at large air masses should be given more weight in turbidity analyses, assuming that the instrumental error does not increase with air mass due to lower signal, misalignment, or obstructions on the horizon. Absolute errors larger than 0.01

TABLE 3. Possible absolute error, $\Delta\delta_a$, caused by a ±20% error in the O_3 and NO_2 amounts, and an error of ±20% or ±100% in w, for the reference w between 0.1 and 5 cm. The first number is for an instrumental error of ±0.5%, and the second (inside brackets) for an instrumental error of ±3%.

Exact w (cm)	Z 10°	30°	60°	80°
Error in w: ±20%				
0.1	0.0068 (0.0299)	0.0061 (0.0263)	0.0040 (0.0153)	0.0020 (0.0056)
0.5	0.0081 (0.0309)	0.0074 (0.0273)	0.0051 (0.0156)	0.0028 (0.0059)
1.5	0.0103 (0.0309)	0.0095 (0.0273)	0.0067 (0.0162)	0.0037 (0.0064)
5.0	0.0145 (0.0325)	0.0135 (0.0289)	0.0097 (0.0177)	0.0052 (0.0073)
Error in w: ±100%				
0.1	0.0318 (0.0431)	0.0294 (0.0390)	0.0213 (0.0260)	0.0118 (0.0129)
0.5	0.0557 (0.0629)	0.0516 (0.0576)	0.0373 (0.0401)	0.0208 (0.0214)
1.5	0.0811 (0.0862)	0.0752 (0.0794)	0.0547 (0.0566)	0.0306 (0.0310)
5.0	0.1223 (0.1258)	0.1136 (0.1164)	0.0826 (0.0839)	0.0458 (0.0461)

optical depth are a potential problem in clean dry climates such as mountainous areas where δ_a is already very low and where it may be difficult to accurately estimate w. Also, relatively large errors may be encountered if w is itself incorrectly estimated. This topic is discussed further in the following section.

6. Experimental test of the method

An evaluation of the accuracy of the proposed approach is considered important and a necessary step prior to its adoption. It is stressed that such an experimental test appears to have never been attempted with previous methods so that all published broadband turbidity ''data'' have, in fact, unknown accuracy and significance. For the present experimental test, high-quality measurements of both broadband and spectral irradiance from different sites under very different atmospheric conditions have been gathered, along with the necessary coincident meteorological data. For reasons explained in the introduction, the spectral optical depth data obtained from either spectroradiometers or sunphotometers are considered here, the reference values against which the broadband optical depth predictions are tested. It is stressed that any determination of turbidity or aerosol extinction from broadband irradiance data is obtained after the water vapor contribution to atmospheric extinction is removed. Any underestimation of precipitable water automatically results in an overestimation of turbidity or vice versa. This explains why, in what follows, the study of turbidity and precipitable water will be tied together.

a. Hazy/humid conditions

A hazy summer day in Cape Canaveral, Florida (latitude 28°25′N, longitude 80°36′W, altitude 2 m), is investigated using 5-min averaged data of broadband irradiance, pressure, air temperature, and dewpoint temperature measured at the Florida Solar Energy Center. Direct irradiance is measured with an Eppley NIP, regularly calibrated against an active cavity pyrheliometer traceable to the international reference standards from NOAA and WMO. Cloudiness was observed, and only data before 1100 LST could be used because of increased cloudiness and an almost constantly obscured sun later in the day. The total ozone column (0.308 atm cm) was measured with a Dobson spectrophotometer in Tallahassee, Florida. Precipitable water was stable and close to the average for July, 4.3 cm (Gueymard 1993), according to the twice-daily radiosonde data obtained from the nearby Kennedy Space Center. The 5-min values of precipitable water were calculated from ground-level data of temperature and humidity (Gueymard 1994a) and were in close agreement with the radiosonde data. The total NO_2 column was assumed constant at a relatively low value of 0.5 matm cm at this relatively unpolluted site. Spectral irradiance, obtained with a LiCor portable spectroradiometer, was used to evaluate the ''observed'' values of α and β. The characteristics of this instrument are detailed elsewhere (Myers 1989; Riordan et al. 1989a). The SMARTS2 code was run to predict the output of this instrument if no aerosol was present, using the instrument's specific bandwidth (6.15 nm) and a Gaussian smoothing function. The spectral AOD was then simply obtained from the apparent aerosol transmittance that is calculated as the ratio between the measured irradiance and the predicted irradiance for no aerosol. Log–log plots were obtained for the four available spectral scans (Fig. 10). These plots show a remarkable linearity and an increase in both negative slope (i.e., α) and intercept at 1 μm (i.e., β) with time. Gaps in these plots correspond to regions where strong gaseous absorption occur or where the spectroradiometer's uncertainty becomes too high (Myers 1989; Riordan et al. 1989a). Figure 11 reveals good agreement between the predictions of β and their observed values. This test day shows a rather high average β (around 0.25), significantly higher than the long-term average for July (0.165), which was estimated for this site (Gueymard 1993). Circumsolar radiation appears to have only a small but discernible effect in this case (Fig. 10).

b. Average conditions

Measurements obtained for 4 June 1992 at Albany, New York (latitude 42°42′N, longitude 73°50′W, altitude 79 m), include broadband irradiance, temperature, and relative humidity, so that precipitable water could be estimated from Gueymard's method (1994a). Estimates of w varied from 2.39 to 2.54 cm during the cloudless part of the day for which spectral data were also available, and these values are comparable to the long-term average for June calculated with the same method (Gueymard 1994a). Spectral irradiance was recorded with an MFRSR instrument (Harrison et al. 1994), and this dataset was preprocessed with the ''objective algorithms'' method (Harrison and Michalsky 1994). For the present test, constant O_3 and NO_2 total abundances of 0.3 and 0.0005 atm cm, respectively, were assumed.

Spectral aerosol optical depth data at 415, 500, 610, 665, and 862 nm were obtained from the measured total optical depths by removing the corresponding contributions of all other atmospheric extinction processes predicted by SMARTS2 at these wavelengths. The instantaneous values of α and β were obtained from a fit of these aerosol optical depths against the Ångström equation. This analysis showed that, until 1000 LST, α was stable and almost constant at about 1.2, which is close to the conventional value of 1.3. Also, β was found to be very stable during the measurement period. The comparison between the predicted and measured values of β appears in Fig. 12 and shows good overall correspondence, considering that the exact total abundances

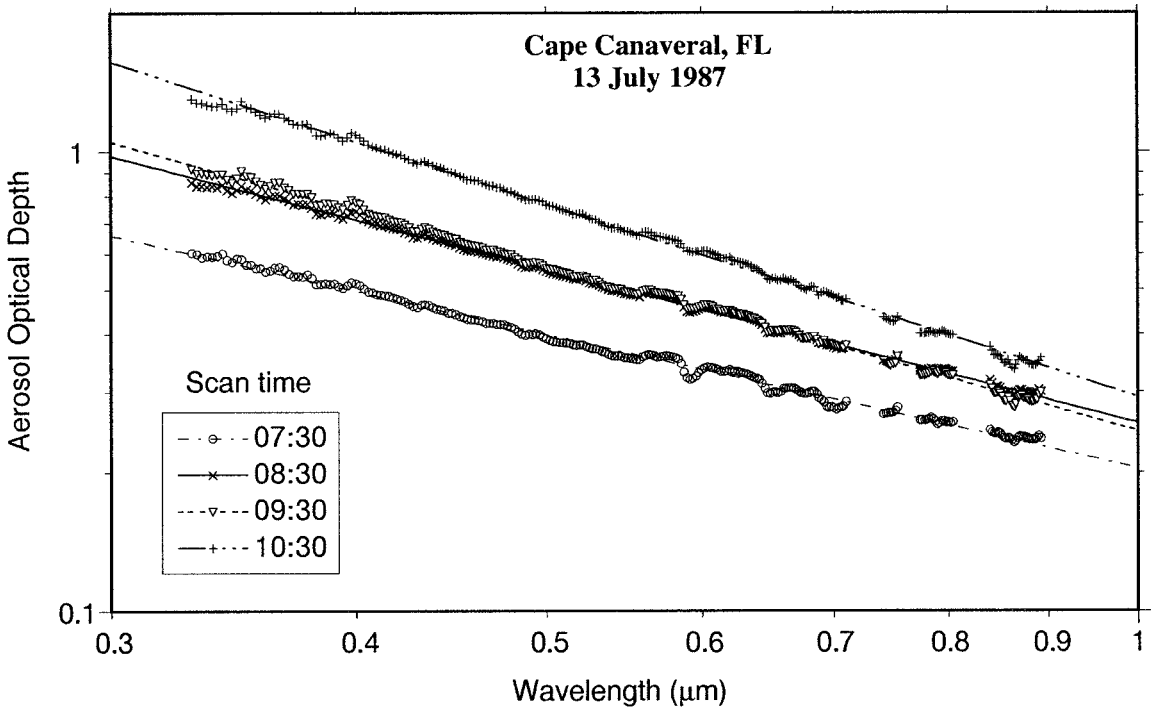

FIG. 10. Spectral aerosol optical depth measured at Cape Canaveral, Florida, with a spectroradiometer.

of H_2O, NO_2, and O_3 were not known. Error bars indicate the resulting possible variation in β when the calculated precipitable water is varied by $\pm 20\%$. All except the two extreme observed data points fall within these limits.

c. Clean dry conditions

Data from three different sites are analyzed here. First, Welby, Colorado (latitude 39°48′N, longitude 104°54′W, altitude 1555 m), is within the Denver agglomeration, about 10 km northeast of downtown Denver. Winter pollution and temperature inversions are frequent there, leading to dense smog (or ''brown cloud'') occurrences with high concentrations of NO_2. The first test day, D1 (afternoon of 30 November 1987), had moderate smog, while the second test day, D2 (morning of 25 February 1988), had an early moderate smog later decreasing to clear conditions (Riordan et al. 1989b). Although no measurements of the total NO_2 column are available, ground-level NO_2 concentration data are provided for D1 (12 ppb) (Riordan et al. 1989b), giving some indirect indication about the total column abundance under such conditions. It was estimated at a constant 2.4 matm cm for D1, and at a decreasing 2–0.7 matm cm for D2. An Eppley NIP measured the broadband direct irradiance, while the atmospheric optical depth at 380, 500, 860, and 942 nm was obtained with a Sonotek sunphotometer. The total ozone column thickness was measured with a Brewer spectrophotometer at Boulder, about 35 km northwest of Welby (0.301 and 0.267 atm cm for D1 and D2, respectively). Precipitable water was obtained with the 942-nm channel of the sunphotometer, using the 860-nm channel optical depth to estimate the AOD at 942 nm (Bruegge et al. 1992). Alternate determinations of w were made from ground-level measurements of temperature and humidity. Twice-daily radiosonde data from the nearby Stapleton

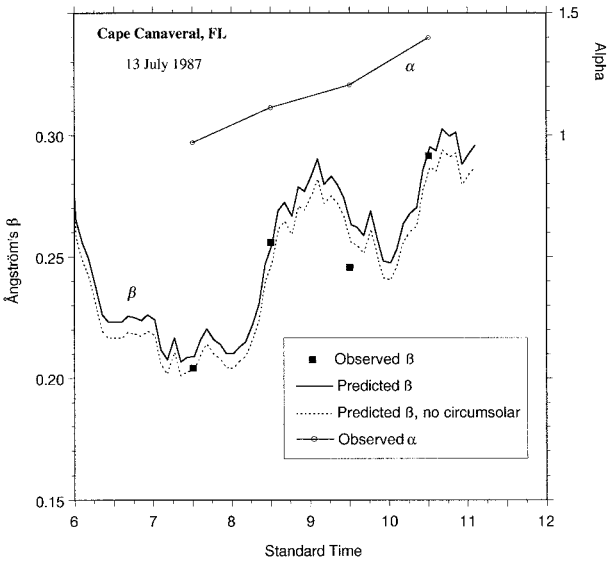

FIG. 11. Predicted vs observed β turbidity coefficient at Cape Canaveral, Florida. The predicted β is obtained from (15), (18), and (21). The observed α is also plotted (upper part).

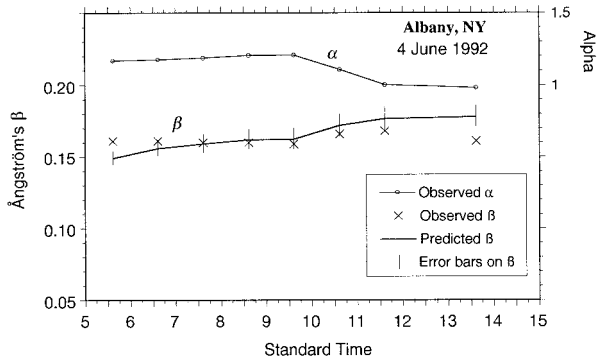

FIG. 12. Predicted [with (15), (18), and (21)] vs observed β turbidity coefficient at Albany, New York. The observed α is also plotted (upper part).

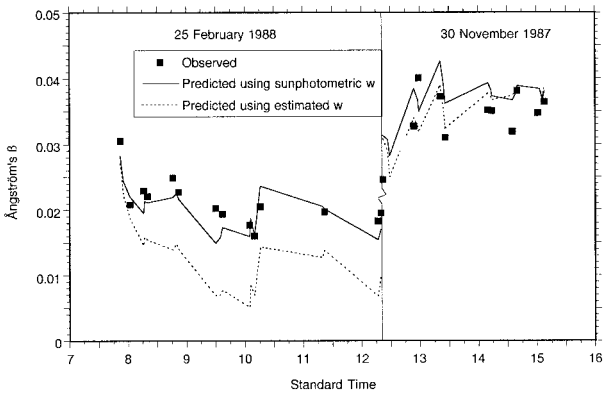

FIG. 13. Predicted [with (15), (18), and (21)] vs observed β turbidity coefficient at Welby, Colorado, for 2 test days and an assumed $\alpha = 1.3$. Precipitable water is either measured with a sunphotometer or estimated from surface conditions.

airport were also obtained. With only three sunphotometer channels left for the determination of AOD (using SMARTS2 as before for the reduction process), log–log plots of AOD versus wavelength were not expected to provide an accurate determination of α (Cachorro et al. 1987a). Nevertheless, a linear fit of these data points showed that α certainly remained close to 1.3, so that the predictions of (15) and (18) were used without any further correction for the real value of α. The observed value of β was obtained by fitting these AODs to the Ångström equation with this fixed value of α, while the 500-nm AOD was given double its normal weight due to its relative importance (this wavelength is close to the peak of the spectrum).

Comparisons between these turbidity observations and predictions from (15) and (18) are shown in Fig. 13. The exaggerated sawtooth shape of the predicted turbidity curve is caused by the sporadic measurement record. Predictions for precipitable water determined from the sunphotometric method, or from the surface temperature and humidity data (Gueymard 1994a), are both shown. Good agreement between these two concurrent determinations was obtained for D1, when w increased between 0.31 and 0.59 cm. However, poor agreement was obtained for D2. Consequently, β was underpredicted, when using w determined from surface data, by about 0.01 optical depth unit during most of the test period. This translates into a 50% error in β. During the morning of D2, the sunphotometric determinations led to a range of w decreasing from 0.40 to 0.15 cm, whereas its estimates from surface data varied between 0.64 and 0.29 cm. Other empirical methods were also tried to estimate w, but their disagreements were even larger. For example, Reitan's equation (Reitan 1963) predicted a range from 0.73 to 0.42 cm, causing unrealistic β values decreasing from 0.02 to 0.001. The early morning (0500 LST) radiosonde launch gave a value of 0.3 cm. However, this single value cannot be used with complete confidence due to the observed variations of w throughout the day and the likely inhomogeneity in the horizontal and vertical distributions of water vapor. (The launch site is about 10 km away from the experimental site.)

A similar analysis was undertaken with data from the National Renewable Energy Laboratory research facility at Golden, Colorado (latitude 39°42′N, longitude 105°12′W, altitude 1829 m). This site is semirural, 23 km west-southwest of Welby. Since it is also 274 m higher than Welby, it is typically above the Denver inversion layer, thus enjoying a cleaner and dryer atmosphere. The same experimental procedure used in Welby was transported to Golden for a unique test day on 26 February 1988 (the day after D2 at Welby). The sunphotometric data during that morning showed an almost constant value of w at about 0.15 cm. In contrast, a large range of w estimates, from about 0.05 to 0.45 cm, were obtained with 11 different empirical formulas tested here (Bolsenga 1965; Garrison and Adler 1990; Gates 1962; Gueymard 1994a; Idso 1969; Leckner 1978; McGee 1974; Myers and Maxwell 1992; Reitan 1963; Smith 1966; Won 1977) using only surface data. Such discrepancy between the ''true'' instantaneous water vapor column and its estimate from surface data is normal due to frequent departures of the actual water vapor vertical profile from its assumed average profile (Reber and Swope 1972; Schwarz 1968). In the present case, about half of the empirical methods tend to overestimate precipitable water, leading to underpredictions in β, if not nonphysical negative values. Another potential source of error is simply due to the fact that relative humidity is sometimes difficult to measure accurately, especially under very dry conditions. This seems to be the cause of the discrepancy observed here during the test day in Golden. The measured relative humidity was always less than or equal to 5% at the precise moment when each of the 11 empirical w estimates had a noticeable dip, that is, during the periods 0845–1015 and 1045–1200 LST. The measurement uncertainty of the instrument used here was estimated at ± 2 counts (Riordan et al. 1990). Thus, a 100% relative error in relative

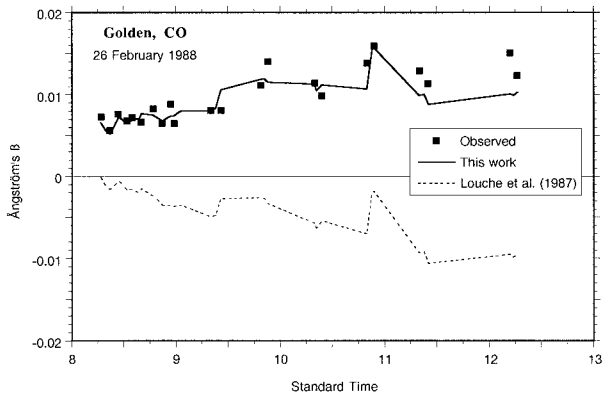

FIG. 14. Predicted [with (15), (18), and (21)] vs observed β turbidity coefficient at Golden, Colorado, for a winter test day and an assumed $\alpha = 1.3$. Results from the Louche method (1987) are also shown.

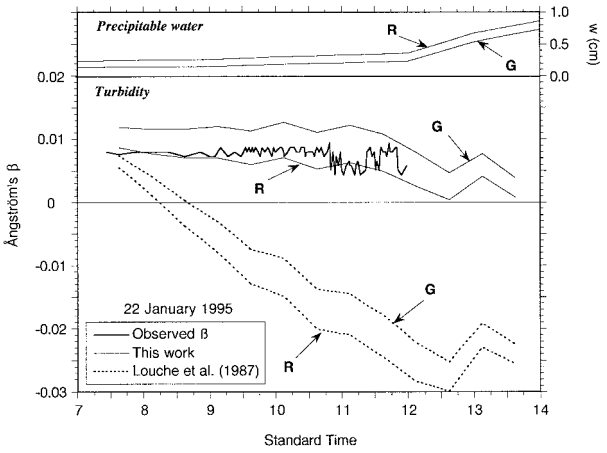

FIG. 15. Predicted [with (15), (18), and (21)] vs observed β turbidity coefficient at Mauna Loa, Hawaii, for a winter test day, an assumed $\alpha = 1.3$, and two different determinations precipitable water (top box): (G) using Gueymard's method (1994) and (R) using Reitan's method (1963). Results from the Louche method (1987) are also shown.

humidity—and thus in w—was quite possible when it was recorded as only 2% between 0900 and 1000 LST. More generally, this measurement accuracy problem is of considerable importance in dry environments because empirical calculations of w are based on its proportionality to the surface relative humidity. As shown in Table 3, a 100% error in w translates into a large uncertainty in δ_a and thus in β.

Using the sunphotometric determinations of w, the predicted β values are found to agree well with the observed values, which were relatively stable at around 0.01 (Fig. 14). As mentioned earlier, any significant error in E_{bn}, w, or in the parameterization may cause the predicted β to be negative. The latter cause appears to be the case for the predictions of Louche's method (Louche et al. 1987), also shown in Fig. 14 (the same input data were used for both methods). In the Louche method, the aerosol transmittance is first calculated as

$$\tau_a = (E_{bn}/E_{0n})/(k\tau_R\tau_o\tau_g\tau_w), \qquad (23)$$

where k is a fixed coefficient with a value of 0.9751 according to Louche et al. (1987) and 0.9662 according to the original radiation model on which this method is based (Bird and Hulstrom 1981). Using the Louche method, the predictions of the product $\tau_R\tau_o\tau_g$ are very close to those of τ_c from (6) and (9). Similarly, the predictions of τ_w by this method are very close to those of τ_w from (10) and (A1) in the appendix. It follows that the main reason for the negative predictions of the Louche method is the very presence of k in (23). The original authors introduced it to correct for the incomplete transmitted spectrum when compared to its extraterrestrial counterpart (i.e., 0.3–3 μm versus 0–∞). This appears to be a redundant correction, considering that the transmitted spectrum is reduced through scattering and absorption processes that are duly accounted for in τ_R, τ_o, τ_g, and τ_w. This inherent double correction in this model is such that τ_a frequently becomes larger than 1 in (23) under very dry and clean atmospheric conditions. This problem is apparently compounded with the inaccuracy of calculating β from τ_a in the Louche method (Fig. 9).

The last dataset to be investigated was measured at the Mauna Loa Observatory (MLO), Hawaii (latitude 19°32′N, longitude 155°34′W, altitude 3398 m). The available test day (22 January 1995, morning) represents typical conditions of low tropospheric aerosol and normal stratospheric background aerosol. Direct irradiance data were available every 3 min, whereas continuous 1-min reduced values of AOD were obtained from a ''PMOD-type'' three-channel sunphotometer. However, only data from the 380- and 778-nm channels were available for this test day. The AODs at these wavelengths show remarkable stability during the test period, especially before 1030 LST. This is why MLO is a place of choice for calibrating sunphotometers. The observed β values were extrapolated from the AOD at 778 nm, using Ångström's equation and $\alpha = 1.3$ to be consistent with the main assumption of the present method. Also, extrapolating the AOD to 1 μm from data at 380 nm is generally not reliable due to departure from the Ångström idealized model and other problems discussed elsewhere (Cachorro et al. 1989). Values remain roughly constant at about 0.008 with increasing structure after 1030 LST. Turbidity calculations with both the present method and Louche's method were performed only every half-hour. Unfortunately, no onsite determination of w could be obtained so that precipitable water was estimated, and interpolated, from hourly surface data using the methods of Gueymard (1994a) and Reitan (1963). (Preliminary tests showed that these methods were reliable at high-altitude sites such as this one.) A typical upward trend of w during the morning hours is apparent in these numbers (top box of Fig. 15), with a noticeable acceleration around 1200. These trends are characteristic of this site and are caused by upward con-

vection along the heated slope of the Mauna Loa volcano, thus bringing moist air from below. For this particular day, Reitan's method consistently predicts about 0.11 cm more precipitable water than Gueymard's method. Although this is a small number in absolute terms, it represents 73% more precipitable water than Gueymard's prediction at 0800 for instance.

Ozone was measured with a Dobson spectrophotometer (0.221 atm cm) and seasonal stratospheric NO_2 was assumed (0.1 matm cm). The turbidity predictions for this day appear in the lower box of Fig. 15. As noted before, for low turbidity conditions, the Louche method predicts negative values most of the time and is thus not suitable for these conditions. Neither determination of precipitable water could improve this behavior. On the other hand, the present method's predictions remain close (within 0.004) to the observed values. Reitan's estimate of w seems to improve the estimates of β until about 1130 LST, but thereafter β is underestimated. Other factors may obviously explain these slight differences, but the exercise shows that extremely accurate and detailed datasets are needed to test broadband turbidity determinations, especially when clean dry conditions are encountered. It is hoped that such datasets will be obtained to test this method for longer periods under an even larger variety of atmospheric conditions.

d. Mean monthly turbidity from hourly irradiances

In many cases, only *hourly* average irradiances from network-operated radiation stations are available to the experimenter. Many studies have reported results of monthly average broadband turbidity over long periods of time predicted from such data (e.g., Fox 1994; Freund 1983; Garrison and Sahami 1995; Gueymard and Garrison 1998; Hay and Darby 1984; Kambezidis et al. 1993; Polavarapu 1978; Uboegbulam and Davies 1983; Yamashita 1974). The same approach is followed here, using measured pyrheliometric data from the NSRDB (Maxwell et al. 1991; Maxwell et al. 1995). Two U.S. stations with widely different aerosol regimes are considered here: Burns, Oregon (latitude 43°35′N, longitude 119°03′W, altitude 1271 m), a high-altitude site with normally clean dry, cloudy winters and sunny summers, and Miami, Florida (latitude 25°48′N, longitude 80°16′W, altitude 2 m), a sea level site with a relatively clean and clear atmosphere in winter turning into hazy, humid, and cloudy skies in summer. The periods of measurements were from April 1979 to December 1981 for Burns, and April 1978 to December 1981 for Miami (with an 8-month interruption at the latter site). These periods were selected as corresponding to the best available irradiance data according to Maxwell et al. (1995). Clear hours were selected from hourly observations of cloud cover at both sites, following a procedure similar to what was used during the development of the NSRDB (Maxwell et al. 1995). Because these cloud observations are made at some distance of the radiation station and are only spot and subjective observations, sudden spikes of predicted turbidity during a day were interpreted as due to the passage of small clouds and were therefore eliminated from the analysis. The difficulty of defining clear hours a posteriori without any continuous objective cloud observations is obviously a limitation, which also applies to all studies of this type. But it is argued that, when dealing with monthly average values, the turbidity overestimation due to unaccounted cloud passages may be counterbalanced, at least in part, by underestimations due to the underrepresentration of hazy days under partly cloudy conditions.

No spectrally determined reference data were available in this case. Predictions of broadband aerosol optical depth (or Unsworth–Monteith turbidity coefficient) from the present method were simply compared to those of Maxwell's method (Maxwell et al. 1995) and of Louche's method (Louche et al. 1987) using the same precipitable water and ozone data as in the NSRDB. [Other monthly mean precipitable water estimates, according to Garrison and Adler (1990), Gueymard (1994a), Leckner (1978), and Myers and Maxwell (1992), were very close to each other and to the NSRDB values; because it was also found that the mean monthly turbidities were not affected by these small differences—a result found for other stations too by Gueymard and Garrison (1998)—only the turbidity evaluated with one published precipitable water dataset are discussed here.] The results, which appear in Fig. 16 for Burns and Fig. 17 for Miami, indicate that the Maxwell and Louche methods predict almost identically, which could be expected because their methodologies are almost identical. They also consistently overpredict δ_a at both sites by about 10% compared to the present method. This difference cannot be attributed to anything else than the different approach used in the present method. Curiously, this does not translate into a similar difference when comparing Louche's predictions of Ångström's β to those of the present method, despite the fact that they are both calculated from δ_a. (Maxwell's method does not predict β.) Whereas Louche's predictions of β are about 11% lower at Burns, they are 2% higher at Miami. This behavior may be caused by inconsistencies in Louche's method, as shown in Fig. 9. This finding also suggests that the numerous turbidity estimates based on Louche's method may need to be corrected in some cases.

7. Conclusions

An extended methodology has been presented to accurately calculate broadband turbidity. It can provide useful information on the total atmospheric extinction due to the aerosol column using only common broadband pyrheliometric measurements of direct-beam radiation. Because no spectral input is involved, the method is easy to implement but also limited in its scope (no information on spectral dependence of the aerosol optical depth can be obtained directly). The method is physical in nature because it does not involve any em-

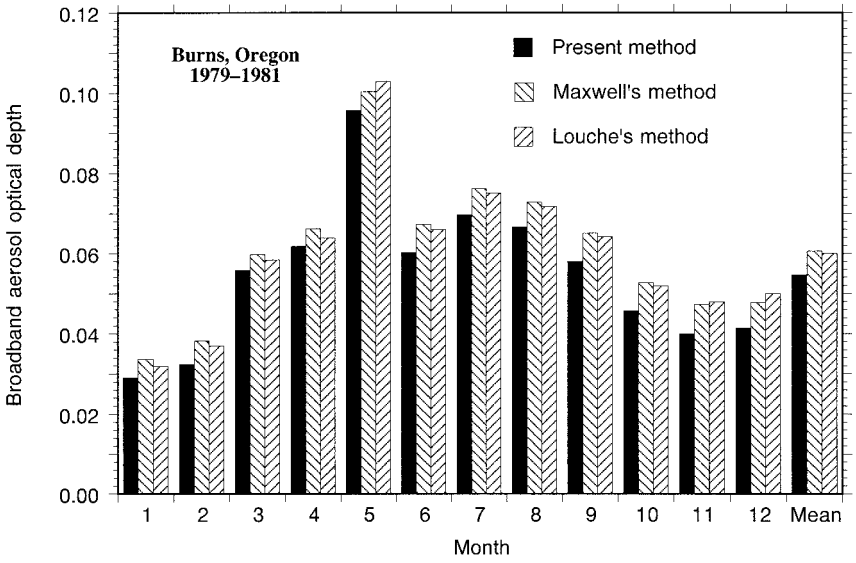

FIG. 16. Predicted mean monthly broadband aerosol optical depth (BAOD) for Burns, Oregon, using the present method (15) and those of Maxwell et al. (1995) and Louche et al. (1987).

pirical relationship, contrary to most previous methods. It is based on spectral calculations using an improved extraterrestrial spectrum and an updated irradiance model. The spectral integration is performed with multilayer-weighted functions matching the altered spectrum above each atmospheric extinction layer. In particular, the aerosol broadband optical depth was successfully parameterized despite its complex dependence on β, m_a, and w. An important outcome of the proposed method is that *all four* widely used turbidity coefficients (Ångström, Linke, Schüepp, and Unsworth–Monteith) can be easily interrelated without the use of any empirical relation, thus providing a consistent way to compare data expressed in different ways. The Unsworth–Monteith coefficient (or broadband aerosol optical depth) is found to depend slightly on both zenith angle and water vapor, so that caution is needed when comparing data from different parts of a day or year. The Linke coefficient depends slightly on zenith angle but considerably on water vapor, so that its use is not recommended in aerosol climatology studies. A correction for the parasitic effect of circumsolar radiation is proposed for different pyrheliometer geometries. The Ångström and Schüepp coefficients depend only on aerosol and represent the

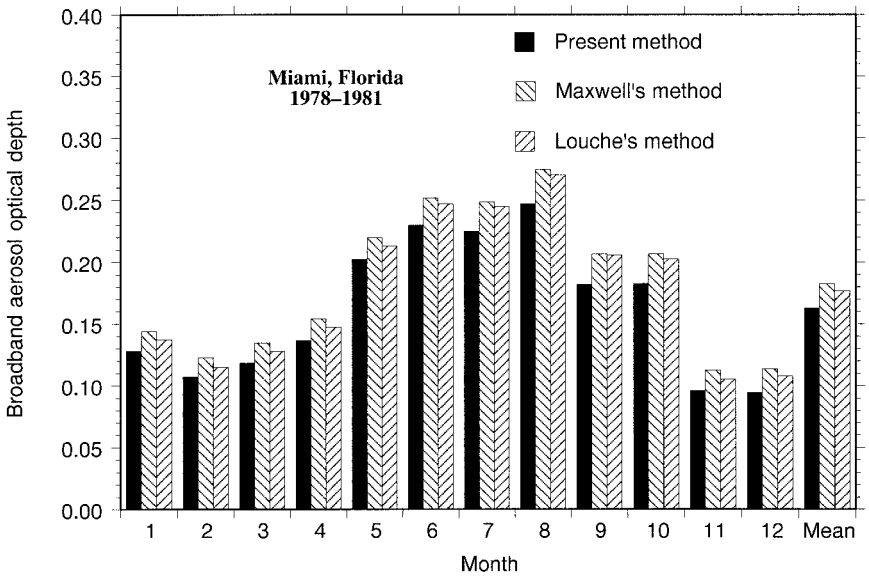

FIG. 17. Predicted mean monthly broadband aerosol optical depth (BAOD) for Miami, Florida, using the present method (15) and those of Maxwell et al. (1995) and Louche et al. (1987).

turbidity coefficients of choice in such studies. It is also shown that aerosol turbidity may be significantly overestimated if NO_2 absorption is neglected, as is commonly done.

A preliminary evaluation of the method indicates good overall agreement with high-quality irradiance and optical depth data. Whereas the parameterization process is not likely to contribute to any significant error in the predicted turbidity, other possible sources of error have been investigated in detail. The most important are the errors in irradiance measurement and the induced error due to an incorrect preliminary estimation of precipitable water if it is not measured coincidentally. In particular, precipitable water estimates based on surface data of relative humidity may lead to significant error in instantaneous or short-term data. These latter sources of error decrease sharply with increasing zenith angle, so that the method should be employed preferably at large air masses. Tests under hazy or moderately turbid skies confirm the validity of the method, although these tests should be repeated for a larger number of days. However, the possible relative error of the method increases when turbidity decreases, so that reliable predictions are conditional upon the accuracy of both direct irradiance and precipitable water data. Under extreme atmospheric conditions, such as the very clean and dry mountain skies, the present method still provides reasonable estimates of turbidity, whereas an earlier method (Louche et al. 1987) often predicts unrealistically low or negative turbidity values. Overall, the different tests indicate that the present method can be used to accurately predict turbidity when the appropriate atmospheric conditions are known with sufficient accuracy. Provided that these conditions are met (particularly, a good accuracy on precipitable water), this method can be applied to supplement spectrally based determinations of turbidity through the use of large databases of direct irradiance that are available throughout the world.

Acknowledgments. The author thanks Ellsworth Dutton, Joe Michalsky, and Benoît Molineaux for providing some of the measured data. Paul Jindra and Helen Power were particularly instrumental in reviewing the different versions of this manuscript.

APPENDIX

Calculation of δ_c, δ_w, and δ_a

The clean dry atmosphere optical depth is parameterized with

$$\delta_c = f_1(p, m_R)\,[f_2(u_o, m_R) + f_3(m_R)] + f_4(u_o, m_R) + f_5(u_n, m_R),$$

where f_1, f_2, f_3, f_4, and f_5 are simple functions whose coefficients are obtained by fitting the numerical data with a least squares technique. Defining $q = 1 - p/p_0$, where $p_0 = 1013.25$ mb, the following parameterizations are proposed.

$$f_1 = (a_0 + a_1 m_R)/(1 + a_2 m_R).$$

$$f_2 = b_0 + b_1 m_R^{0.25} + b_2 \ln(m_R).$$

$$f_3 = (0.19758 + 0.00088585 m_R - 0.097557 m_R^{0.2}) \div (1 + 0.0044767 m_R).$$

$$f_4 = (c_0 + c_1 m_R^{-0.72})/(\exp(1 + c_2 m_R).$$

$$f_5 = u_{ns}[2.8669 - 0.078633 \ln^{2.36}(m_R)].$$

$$a_0 = 1 - 0.98173q.$$

$$a_1 = 0.18164 - 0.24259q + 0.050739q^2.$$

$$a_2 = 0.18164 - 0.17005q - 0.0084949q^2.$$

$$b_0 = -0.0080617 + 0.028303u_o - 0.014055u_o^2.$$

$$b_1 = 0.011318 - 0.041018u_o + 0.023471u_o^2.$$

$$b_2 = -0.0044577 + 0.016728u_o - 0.01091u_o^2.$$

$$c_0 = 0.0036916 + 0.047361u_o + 0.0058324u_o^2.$$

$$c_1 = 0.015471 + 0.061662u_o - 0.044022u_o^2.$$

$$c_2 = 0.039904 - 0.038633u_o + 0.054899u_o^2.$$

Similarly, the broadband water vapor optical depth is obtained from

$$\delta_w = M[g_1 + g_2 M m_w + g_3 (M m_w)^{1.28}] \div (1 + g_4 M m_w), \quad \text{(A1)}$$

where m_w is calculated from (8b) and the following parameterizations are given.

$$M = (1.7135 + 0.10004 m_w + 0.00053986 m_w^2) \div (1.7149 + 0.097294 m_w + 0.002567 m_w^2).$$

$$g_1 = (\gamma_1 w + \gamma_2 w^{1.6})/(1 + \gamma_3 w).$$

$$g_2 = (\varphi_1 w + \varphi_2 w^{1.6})/(1 + \varphi_3 w).$$

$$g_3 = (\kappa_1 w + \kappa_2 w^{1.6})/(1 + \kappa_3 w).$$

$$g_4 = (\nu_1 w + \nu_2 w^{0.62})/(1 + \nu_3 w + \nu_4 w^2).$$

$$\gamma_1 = 1.728 - 2.1451q)/(1 - 0.96212q).$$

$$\gamma_2 = (0.37042 + 0.64537q)/(1 + 0.94528q).$$

$$\gamma_3 = (3.5145 - 0.12483q)/(1 - 0.34018q).$$

$$\varphi_1 = (0.63889 - 0.81121q)(1 - 0.79988q).$$

$$\varphi_2 = (0.06836 + 0.49008q)/(1 + 4.7234q).$$

$$\varphi_3 = (2.1567 + 1.4546q)/(1 + 0.038808q).$$

$$\kappa_1 = (-0.1857 + 0.23871q)/(1 - 0.84111q).$$

$$\kappa_2 = (-0.022344 - 0.19312q)/(1 + 6.2169q).$$

$$\kappa_3 = (2.1709 + 1.6423q)/(1 + 0.062545q).$$

$$\nu_1 = 3.3704 + 6.8096q.$$

$$\nu_2 = (12.487 - 18.517q - 0.4089q^2) \div (1 - 1.4104q).$$

$$\nu_3 = (2.5024 - 0.56834q - 1.4623q^2) \div (1 - 1.0252q).$$

$$\nu_4 = (-0.030833 - 1.172q - 0.98878q^2) \div (1 + 31.546q).$$

Finally, the broadband aerosol optical depth is obtained as

$$\delta_a = \beta(s_1 + s_2\beta).$$

where, for $\alpha = 1.3$,

$$s_1 = (d_0 + d_1 m_a)/(1 + d_2 m_a),$$

$$s_2 = (h_0 + h_1 m_a + h_2 m_a^2)/(1 + h_3 m_a^n),$$

$$d_0 = (1.6685 + 4.1257w + 0.018748w^2) \div (1 + 2.336w),$$

$$d_1 = (0.075379 + 0.066532w - 0.0042634w^2) \div (1 + 1.9477w),$$

$$d_2 = (0.12867 + 0.24264w - 0.0087874w^2) \div (1 + 3.3566w),$$

$$h_0 = (-0.032335 - 0.0060424w)/(1 + 0.023563w),$$

$$h_1 = (-0.38229 - 0.0009926w)/(1 + 0.044137w^{0.594}),$$

$$h_2 = (-0.0059467 + 0.0054054w)/(1 + 0.91487w),$$

$$h_3 = (0.21989 + 0.041897w)/(1 + 0.35717w),$$

and

$$n = (1.3211 + 2.2036w)/(1 + 1.9367w).$$

REFERENCES

Abdelrahman, M. A., S. A. M. Said, and A. N. Shuaib, 1988: Comparison between atmospheric turbidity coefficients of desert and temperate climates. *Sol. Energy,* **40,** 219–225.

Al-Jamal, K., S. Ayyash, M. Rasas, S. Al-Aruri, and N. Shaban, 1987: Atmospheric turbidity in Kuwait. *Atmos. Environ.,* **21,** 1855–1859.

Anderson, G. P., S. A. Clough, F. X. Kneizys, J. H. Chetwynd, and E. P. Shettle, 1986: AFGL atmospheric constituent profiles (0–120 km). Tech. Rep. AFGL-TR-86–0110, 43 pp. [Available from Air Force Geophysics Lab., Hanscom AFB, MA 01731.].

——, and Coauthors, 1993: MODTRAN2: Suitability for remote sensing. *Proc. Atmospheric Propagation and Remote Sensing II,* Orlando, FL, SPIE, 514–525.

Ångström, A., 1929: On the atmospheric transmission of sun radiation and on dust in the air. *Geogr. Annal.,* **2,** 156–166.

——, 1961: Radiation to actinometric receivers in its dependence on aperture conditions. *Tellus,* **13,** 425–431.

——, 1970: On determination of the atmospheric turbidity and their relation to pyrheliometric measurements. *Advances in Geophysics,* Vol. 14, Academic Press, 269–284.

——, and B. Rodhe, 1966: Pyrheliometric measurements with special regard to the circumsolar radiation. *Tellus,* **18,** 25–33.

Bergstrom, R. W., and J. T. Peterson, 1977: Comparison of predicted and observed solar radiation in an urban area. *J. Appl. Meteor.,* **16,** 1107–1116.

Berk, A., L. S. Bernstein, and D. C. Robertson, 1989: MODTRAN: A moderate resolution model for LOWTRAN7. Tech. Rep. GL-TR-89–0122, 38 pp. [Available from Air Force Geophysics Lab., Hanscom, MA, 01731.]

Bevington, P. R., 1969: *Data Reduction and Error Analysis for the Physical Sciences.* McGraw–Hill, 336 pp.

Bird, R. E., and R. L. Hulstrom, 1981: Review, evaluation, and improvement of direct irradiance models. *Trans. ASME: J. Sol. Energy Eng.,* **103,** 182–192.

——, and C. Riordan, 1986: Simple solar spectral model for direct and diffuse irradiance on horizontal and tilted planes at the earth's surface for cloudless atmospheres. *J. Climate Appl. Meteor.,* **25,** 87–97.

Blättner, W., 1983: Utilization instruction for the BRITE Monte-Carlo procedure. Res. Note RRA-N8303, 104 pp. [Available from Radiation Research Associates, Fort Worth, TX, 76107.]

Bolsenga, S. J., 1965: The relationship between total atmospheric water vapor and surface dew point on a mean daily and hourly basis. *J. Appl. Meteor.,* **4,** 430–432.

Box, M. A., and A. Deepak, 1979: Atmospheric scattering corrections to solar radiometry. *Appl. Opt.,* **18,** 1941–1949.

——, and ——, 1981: An approximation to multiple scattering in the earth's atmosphere: Almucantar radiance formulation. *J. Atmos. Sci.,* **38,** 1037–1048.

Braslau, N., and J. V. Dave, 1973: Effect of aerosols on the transfer of solar energy through realistic model atmospheres. *J. Appl. Meteor.,* **12,** 601–619.

Bruegge, C. J., J. E. Conel, R. O. Green, J. S. Margolis, R. G. Holm, and G. Toon, 1992: Water vapor column abundance retrievals during FIFE. *J. Geophys. Res.,* **97**(D), 18 759–18 768.

Cachorro, V. E., J. L. Casanova, and A. M. de Frutos, 1987a: The influence of Ångström parameters on calculated direct spectral irradiances at high turbidity. *Sol. Energy,* **39,** 399–407.

——, A. M. de Frutos, and J. L. Casanova, 1987b: Determination of the Ångström turbidity parameters. *Appl. Opt.,* **26,** 3069–3076.

——, M. J. Gonzalez, A. M. de Frutos, and J. L. Casanova, 1989: Fitting Ångström's formula to spectrally resolved aerosol optical thickness. *Atmos. Environ.,* **23,** 265–270.

Cañada, J., J. M. Pinazo, and J. V. Bosca, 1993: Determination of Ångström's turbidity coefficient at Valencia. *Renew. Energy,* **3,** 621–626.

CSAGI, 1957: Radiation instruments and measurements. *Annals of the International Geophysical Year, Instruction Manual,* Pergamon Press, 463 pp.

Cuomo, V., F. Esposito, G. Pavese, and C. Serio, 1993: Determining Ångström's turbidity coefficients—An analysis with a wide-range grating spectrometer. *Aerosol Sci. Tech.,* **18,** 59–69.

Daumont, D., J. Brion, J. Charbonnier, and J. Malicet, 1992: Ozone UV spectroscopy I: Absorption cross-sections at room temperature. *J. Atmos. Chem.,* **15,** 145–155.

Davidson, J. A., C. A. Cantrell, A. H. McDaniel, R. E. Shetter, S. Madronich, and J. G. Calvert, 1988: Visible-ultraviolet absorption cross sections for NO_2 as a function of temperature. *J. Geophys. Res.,* **93**(D), 7105–7112.

Dogniaux, R., 1986: The estimation of atmospheric turbidity. *Proc. Advances in European Solar Radiation Climatology,* London, United Kingdom, U.K. Int. Sol. Energy Soc., 3.1–3.4.

——, Ed., 1994: *Prediction of Solar Radiation in Areas with a Specific Microclimate.* Kluwer, 107 pp.

Dutton, E. G., P. Reddy, S. Ryan, and J. J. DeLuisi, 1994: Features and effects of aerosol optical depth observed at Mauna Loa, Hawaii: 1982–1992. *J. Geophys. Res.,* **99**(D), 8295–8306.

Feussner, K., and P. Dubois, 1930: Trübungsfaktor, precipitable water, Staub. *Gerlands Beitr. Geophys.,* **27,** 132–175.

Fox, J. D., 1994: Calculated Ångström's turbidity coefficients for Fairbanks, Alaska. *J. Climate,* **7,** 1506–1512.

Freund, J., 1983: Aerosol optical depth in the Canadian Arctic. *Atmos.–Ocean,* **21,** 158–167.

Garrison, J., 1995: An evaluation of the effect of volcanic eruption on the solar radiation at six Canadian stations. *Sol. Energy,* **55,** 513–525.

——, and G. P. Adler, 1990: Estimation of precipitable water over the United States for application to the division of solar radiation into its direct and diffuse components. *Sol. Energy,* **44,** 225–241.

——, and K. Sahami, 1995: Analysis of clear hour solar irradiation for seven Canadian stations. *Sol. Energy,* **55,** 505–512.

Gates, D. M., 1962: *Energy Exchange in the Biosphere.* Harper & Row.

Grenier, J. C., A. de la Casinière, and T. Cabot, 1994: A spectral model of Linke's turbidity factor and its experimental implications. *Sol. Energy,* **52,** 303–314.

——, ——, and ——, 1995: Atmospheric turbidity analyzed by means of standardized Linke's turbidity factor. *J. Appl. Meteor.,* **34,** 1449–1458.

Gueymard, C., 1993: Atmospheric turbidity in Florida. Tech. Rep. FSEC-PF-247-93, 7 pp. [Available from Florida Sol. Energy Center, 1679 Clearlake Rd., Cocoa, FL 32922-5703.]

——, 1994a: Analysis of monthly average atmospheric precipitable water and turbidity in Canada and northern United States. *Sol. Energy,* **53,** 57–71.

——, 1994b: Updated transmittance functions for use in fast spectral direct beam irradiance models. *Proc. Sol. '94 Conf.,* San Jose, CA, Amer. Sol. Energy Soc., 355–360.

——, 1995: SMARTS2, a Simple Model of the Atmospheric Radiative Transfer of Sunshine: Algorithms and performance assessment. Tech. Rep. FSEC-PF-270-95, 78 pp. [Available from Florida Sol. Energy Center, 1679 Clearlake Rd., Cocoa, FL 32922-5703.]

——, and J. D. Garrison, 1998: Critical evaluation of precipitable water and atmospheric turbidity in Canada using measured hourly solar irradiance. *Sol. Energy,* in press.

——, and H. D. Kambezidis, 1997: Illuminance turbidity parameters and atmospheric extinction in the visible spectrum. *Quart J. Roy. Meteor. Soc.,* **123,** 679–697.

Harrison, L., and J. J. Michalsky, 1994: Objective algorithms for the retrieval of optical depths from ground-based measurements. *Appl. Opt.,* **33,** 5126–5132.

——, J. Michalsky, and J. Berndt, 1994: Automated multifilter rotating shadow-band radiometer: An instrument for optical depth and radiation measurements. *Appl. Opt.,* **33,** 5118–5125.

Hay, J. E., and R. Darby, 1984: El Chichon—Influence on aerosol optical depth and direct, diffuse and total solar irradiances at Vancouver, B.C. *Atmos.–Ocean,* **22,** 354–368.

Hinzpeter, H., 1950: Über Trübungsbestimmungen in Potsdam in dem Jahren 1946 und 1947. *Meteor.,* **4,** 1.

Horvath, H., 1994: Remarks and suggestions on nomenclature and symbols in atmospheric optics. *Atmos. Environ.,* **28,** 757–759.

Hoyt, D. V., 1975: New calculations of the Linke turbidity coefficient. *Quart J. Roy. Meteor. Soc.,* **101,** 383–385.

IAMAP, 1986: A preliminary cloudless standard atmosphere for radiation computation. Rep. WCP-112, WMO/TD-No. 24, 53 pp. [Available from World Meteorological Organization, Case Postale 2300, CH-1211 Geneva 2, Switzerland.]

Idso, S. B., 1969: Atmospheric attenuation of solar radiation. *J. Atmos. Sci.,* **26,** 1088–1095.

Kambezidis, H. D., D. H. Founda, and N. S. Papanikolaou, 1993: Linke and Unsworth–Monteith turbidity parameters in Athens. *Quart J. Roy. Meteor. Soc.,* **119,** 367–374.

Kasten, F., 1980: A simple parameterization of the pyrheliometric formula for determining the Linke turbidity factor. *Meteor. Rundsch.,* **33,** 124–127.

——, 1988: Elimination of the virtual diurnal variation of the Linke turbidity factor. *Meteor. Rundsch.,* **41,** 93–94.

——, 1996: The Linke turbidity factor based on improved values of the integral Rayleigh optical thickness. *Sol. Energy,* **56,** 239–244.

Katz, M., A. Baille, and M. Mermier, 1982: Atmospheric turbidity in a semi-rural site. Part I: Evaluation and comparison of different atmospheric turbidity coefficients. *Sol. Energy,* **28,** 323–327.

Leckner, B., 1978: The spectral distribution of solar radiation at the Earth's surface—Elements of a model. *Sol. Energy,* **20,** 143–150.

Linke, F., 1922: Transmissions-Koeffizient und Trübungsfaktor. *Beitr. Phys. Atmos.,* **10,** 91–103.

Louche, A., G. Peri, and M. Iqbal, 1986: An analysis of Linke turbidity factor. *Sol. Energy,* **37,** 393–396.

——, M. Maurel, G. Simonnot, G. Peri, and M. Iqbal, 1987: Determination of Ångström's turbidity coefficient from direct total solar irradiance measurements. *Sol. Energy,* **38,** 89–96.

Major, G., 1994: Circumsolar correction for pyrheliometers and diffusometers. Rep. WMO/TD-No. 635, 42 pp. [Available from World Meterological Organization, Case Postale 2300, CH-1211 Geneva, Switzerland.]

Maxwell, E. L., D. R. Myers, M. D. Rymes, T. L. Stoffel, and S. M. Wilcox, 1991: Producing a national solar radiation data base. *1991 Solar Wind Congress,* M. E. Arden, S. M. A. Burley, and M. Coleman, Eds., Pergamon Press, 1007–1012.

——, W. F. Marion, D. R. Myers, M. D. Rymes, and S. M. Wilcox, 1995: National Solar Radiation Data Base—Final Technical Report. Tech. Rep. NREL/TP-463–5784, 289 pp. [Available from National Renewable Energy Laboratory, Golden, CO, 80401-3393.]

McGee, O. S., 1974: A surface dewpoint-precipitable water vapour relationship for South Africa. *South Afr. J. Sci.,* **70,** 119–120.

McGuffie, K., J. G. Cogley, and A. Henderson-Sellers, 1985: Climatological analysis of Arctic aerosol quantity and optical properties at Resolute, N. W. T. *Atmos. Environ.,* **19,** 707–714.

Molineaux, B., and P. Ineichen, 1996: On the broad band transmittance of direct irradiance in a cloudless sky and its application to the parameterization of atmospheric turbidity. *Sol. Energy,* **56,** 553–563.

Myers, D. R., 1989: Estimates of uncertainty for measured spectra in the SERI spectral solar radiation data base. *Sol. Energy,* **43,** 347–353.

——, and E. L. Maxwell, 1992: Hourly estimates of precipitable water for solar radiation models. *Proc. Solar '92,* Cocoa Beach, FL, Amer. Sol. Energy Soc., 317–322.

Pastiels, R., 1959: Contribution à l'étude du problème des méthodes actinométriques. Institut Royal Météorologique Rep. A11, 128 pp.

Polavarapu, R. J., 1978: Atmospheric turbidity over Canada. *J. Appl. Meteor.,* **17,** 1368–1374.

Putsay, M., 1995: Circumsolar radiation calculated for various aerosol models. *Idójárás,* **99,** 67–76.

Rawlins, F., and R. J. Armstrong, 1985: Recent measurements of broad-band turbidity in the United Kingdom. *Meteor. Mag.,* **114,** 89–99.

Reagan, J. A., L. W. Thomason, B. M. Herman, and J. M. Palmer, 1986: Assessment of atmospheric limitations on the determination of the solar spectral constant from ground-based spectroradiometer measurements. *IEEE Trans. Geosci. Remote Sens.,* **GE-24,** 258–266.

Reber, E. E., and J. R. Swope, 1972: On the correlation of the total precipitable water in a vertical column and absolute humidity at the surface. *J. Appl. Meteor.,* **11,** 1322–1325.

Reitan, C. H., 1963: Surface dew point and water vapor aloft. *J. Appl. Meteor.,* **2,** 776–779.

Riordan, C., D. Myers, M. Rymes, R. Hulstrom, W. Marion, C. Jennings, and C. Whitaker, 1989a: Spectral solar radiation data base at SERI. *Sol. Energy,* **42,** 67–79.

——, T. L. Stoffel, and R. L. Hulstrom, 1989b: The effects of urban air pollution on solar radiation. Rep. SERI/TR-215-

3482, 38 pp. [Available from National Renewable Energy Laboratory, Golden, CO, 80401-3393.]

——, D. R. Myers, and R. L. Hulstrom, 1990: Spectral data base documentation. Tech. Rep. SERI/TR-215–3513, 52 pp. [Available from National Renewable Energy Laboratory, Golden, CO 80401-3393]

Roosen, R. G., R. J. Angione, and C. H. Klemcke, 1973: Worldwide variations in atmospheric transmission: 1. Baseline results from Smithsonian observations. *Bull. Amer. Meteor. Soc.*, **54,** 307–316.

Schroeder, R., and J. A. Davies, 1987: Significance of nitrogen dioxide in estimating aerosol optical depth and size distributions. *Atmos.–Ocean,* **25,** 107–114.

Schüepp, W., 1949: Die Bestimmung der Konponenten der atmosphärischen Trübung aus Aktinometer Messungen. *Arch. Meteor. Geophys. Bioklimatol.,* **B1,** 257.

Schwarz, F. K., 1968: Comments on ''Note on the relationship between total precipitable water and surface dew point.'' *J. Appl. Meteor.,* **7,** 509–510.

Shaw, G. E., 1982: Solar spectral irradiance and atmospheric transmission at Mauna Loa Observatory. *Appl. Opt.,* **21,** 2006–2011.

——, J. A. Reagan, and B. M. Herman, 1973: Investigations of atmospheric extinction using direct solar radiation measurements made with a multiple wavelength radiometer. *J. Appl. Meteor.,* **12,** 374–380.

Shettle, E. P., and R. W. Fenn, 1979: Models for the aerosols of the lower atmosphere and the effects of humidity variations on their optical properties. Rep. AFGL-TR-79–0214, 94 pp. [Available from Air Force Geophysics Lab, Hanscom AFB, MA 01731.]

Shiobara, M., J. D. Spinhirne, A. Uchiyama, and S. Asano, 1996: Optical depth measurements of aerosol, cloud, and water vapor using sun photometers during FIRE Cirrus IFO II. *J. Appl. Meteor.,* **35,** 36–46.

Smith, W. L., 1966: Note on the relationship between total precipitable water and surface dew point. *J. Appl. Meteor.,* **5,** 726–727.

Stothers, R. B., 1996: Major optical depth perturbations to the stratosphere from volcanic eruptions: Pyrheliometric period, 1881–1960. *J. Geophys. Res.,* **101**(D), 3901–3920.

Szymber, R. J., and W. D. Sellers, 1985: Atmospheric turbidity at Tucson, Arizona, 1956–83: Variations and their causes. *J. Climate Appl. Meteor.,* **24,** 725–734.

Thomason, L. W., R. J. Szymber, and B. M. Herman, 1982: An examination of reduction techniques for determining the Linke turbidity factor. *J. Appl. Meteor.,* **21,** 1524–1527.

Uboegbulam, T. C., and J. A. Davies, 1983: Turbidity in eastern Canada. *J. Climate Appl. Meteor.,* **22,** 1384–1392.

Unsworth, M. H., and J. L. Monteith, 1972: Aerosol and solar radiation in Britain. *Quart J. Roy. Meteor. Soc.,* **98,** 778–797.

——, and H. A. McCartney, 1973: Effects of atmospheric aerosols on solar radiation. *Atmos. Environ.,* **7,** 1173–1185.

Valko, P., 1967: Über den Zusammenhang zwischen Trübungsfaktor und Trübungs koeffizient. *Arch. Meteor. Geophys. Bioklimatol.,* **B15,** 359–375.

Volz, F., 1959: Photometer mit Selen-Photoelement zur spektralen Messung der Sonnenstrahlung und zur Bestimmung der Wellenlängenabhängigkeit der Dunsttrübung. *Arch. Meteor. Geophys. Bioklimatol.,* **B10,** 100–131.

WMO, 1981: Meteorological aspects of the utilization of solar radiation as an energy source. Tech. Note 172, WMO 557, 273 pp. [Available from World Meteorological Organization, Case Postale 2300, CH-1211 Geneva 2, Switzerland.]

Won, T. K., 1977: The simulation of hourly global radiation from hourly reported meteorological parameters—Canadian prairie area. *Proc. Third Annual Conf.,* Edmonton, AB, Canada, Sol. Energy Society of Canada.

Yamamoto, G., M. Tanaka, and K. Arao, 1968: Hemispherical distribution of turbidity coefficient as estimated from direct solar radiation measurements. *J. Meteor. Soc. Japan,* **46,** 278–300.

——, ——, and ——, 1971: Secular variation of atmospheric turbidity over Japan. *J. Meteor. Soc. Japan,* **49,** 859–865.

Yamashita, S., 1974: A comparative study of turbidity in an urban and a rural environment at Toronto. *Atmos. Environ.,* **8,** 507–518.

Young, A. T., 1974: Observational technique and data reduction. *Astrophysics, Pt. A: Optical and Infrared,* Vol. 12, N. Carleton, Ed., Academic Press, 123–192.

Zerlaut, G. A., 1983: Solar radiation measurements: Calibration and standardization efforts. *Advances in Solar Energy,* Vol. 1, K. W. Böer, and J. A. Duffie, Eds., Amer. Sol. Energy Soc., 19–59.